

# CAIRNS: THE CLUSTER AND INFALL REGION NEARBY SURVEY III. ENVIRONMENTAL DEPENDENCE OF H $\alpha$ PROPERTIES OF GALAXIES

KENNETH RINES<sup>1</sup>, MARGARET J. GELLER<sup>2</sup>, MICHAEL J. KURTZ<sup>2</sup>, & ANTONALDO DIAFERIO<sup>3</sup>  
*Draft version April 13, 2018*

## ABSTRACT

We investigate the environmental dependence of star formation in cluster virial regions and infall regions as part of CAIRNS (Cluster And Infall Region Nearby Survey), a large spectroscopic survey of the infall regions surrounding nine nearby rich clusters of galaxies. We use complete, homogeneous spectroscopic surveys of  $K_s$  limited samples in eight of the CAIRNS clusters. Our long-slit spectroscopy yields estimates of star formation rates in environments from cluster cores to the general large-scale structure. Galaxies in infall regions probe whether processes affecting star formation are effective over scales larger than cluster virial regions. The fraction of galaxies with current star formation in their inner disks as traced by H $\alpha$  emission increases with distance from the cluster and converges to the “field” value only at 2-3 virial radii, in agreement with other investigations. However, among galaxies with significant current star formation ( $\text{EW}[\text{H}\alpha] \geq 2\text{\AA}$ ), there is no difference in the *distribution* of  $\text{EW}[\text{H}\alpha]$  inside and outside the virial radius. This surprising result, first seen by Carter et al., suggests that (1) star formation is truncated on either very short timescales or only at moderate and high redshifts or (2) that projection effects contaminate the measurement. We quantify the possible impact of mechanisms which only affect the outer parts of galaxies and thus might not be detected in this survey or any fiber-based survey. The number density profiles of star-forming and non-star-forming galaxies indicate that, among galaxies projected inside the virial radius, at least half of the former and 20% of the latter are “infall interlopers,” galaxies in the infall region but outside the virial region. We show that the kinematics of star-forming galaxies in the infall region closely match those of absorption-dominated galaxies. This result shows that the star forming galaxies in the infall regions are not interlopers from the field and excludes one model of the backplash scenario of galaxy transformation. Finally, we quantify systematic uncertainties in estimating the global star formation in galaxies from their inner disks.

*Subject headings:* galaxies: clusters: general — galaxies: clusters: individual (A119, A168, A194, A496, A539, A1367, A1656(Coma), A2199) — galaxies: kinematics and dynamics — galaxies: fundamental parameters

## 1. INTRODUCTION

One of the most striking features of galaxy clusters at the present epoch is their deficit of late-type galaxies relative to the overall galaxy population in magnitude limited samples. This feature was noted by Hubble & Humason (1931), and eventually quantified by Dressler (1980). Similar trends are seen in galaxy groups (Postman & Geller 1984), suggesting that groups may play an important role in establishing the morphology-density relation. This morphological segregation is reflected in segregation of spectral types, i.e., galaxies in dense environments are much less likely than those in less dense environments to show evidence of ongoing star formation in their spectra (e.g., Salzer 1989; Carter et al. 2001, and references therein). A third method of galaxy classification is to separate them by their broadband colors. Morphology, color, and spectral type are well correlated, but there are galaxies such as “passive spirals” that would be classified differently in these different schemes (Koopmann & Kenney 1998; Goto et al. 2003). Here, we focus on spectral information, in particular H $\alpha$  emission, which traces current star formation.

Recently, several investigators have found that these population differences are not restricted to cluster virial regions. Galaxy properties seem to converge to those of field galaxies only at 2-3 virial radii (Abraham et al. 1996; Balogh et al. 1997; Diaferio et al. 2001; Ellingson et al. 2001; Lewis et al. 2002; Gómez et al. 2003; Balogh et al.

2004; Gray et al. 2004; Tanaka et al. 2004). The two leading explanations for the presence of these galaxies are preprocessing by infalling groups (and/or filaments) and “backplash”. In the backplash model, some galaxies at large radii have passed through the virial region of the cluster and thus may have undergone environmental transformation within the virial radius.

These differences may result from the types of galaxies that form in different environments or from environmental processes (or more likely, some mixture of the two). Truly environmental mechanisms are strongly implicated by the observation that cluster galaxies have different star formation properties than field galaxies with similar stellar mass, morphology, and mean stellar age (Christlein & Zabludoff 2005). Several physical mechanisms can alter star formation in galaxies as they enter dense environments (see Treu et al. 2003, for a clear summary of these mechanisms). Infall regions (where galaxies are infalling onto the main cluster but have not yet reached equilibrium) provide a unique probe of the environmental scale which determines galaxy properties: infall regions are overdense averaged over scales of  $5\text{--}10h^{-1}\text{Mpc}$  (because they are near a cluster) but they contain a wide range of local densities measured on scales of roughly  $1h^{-1}\text{Mpc}$  (e.g., groups and filaments).

Ongoing massive star formation produces H $\alpha$  emission from HII regions. The strength of this emission line is a good measure of the current star formation rate. H $\alpha$  is

relatively insensitive to metallicity, unlike some star formation tracers including [OII] (Kewley et al. 2004). The existence of galaxies with little or no star formation but late-type morphologies suggests that star formation is more sensitive to environment than morphology (van den Bergh 1976; Koopmann & Kenney 1998; Goto et al. 2003; Vogt et al. 2004; Kodama et al. 2004).

Here, we study the H $\alpha$  properties of a large, homogeneous spectroscopic sample of galaxies in the virial regions and infall regions of eight nearby clusters from CAIRNS (The Cluster And Infall Region Nearby Survey, see Rines et al. 2003, hereafter Paper I). This survey is the largest sample of long-slit spectra in cluster infall regions to date. Even with long-slit spectra, the spectral properties are weighted towards those of the inner disks (radii of  $\sim 3$  kpc). Because CAIRNS probes rich clusters, we probe densities up to an order of magnitude larger than studies based on 2dF and SDSS (which at present contain relatively few rich, nearby clusters). The spectroscopic catalogs are complete in the near-infrared to absolute magnitude  $M_{K_s} = -22.7 + 5\log h$  using photometry from 2MASS, the Two-Micron All-Sky Survey (Skrutskie et al. 1997). This limit is approximately one magnitude fainter than  $M_{K_s}^*$ , the characteristic magnitude of the luminosity function averaged over all environments (Cole et al. 2001; Rines et al. 2004). Our selection of galaxies in the near-infrared leads to a sample that is much closer to a sample selected by stellar mass than samples selected at optical wavelengths. Because of the shape of the galaxy luminosity function, a substantial fraction of any magnitude or luminosity limited sample consists of galaxies close to the faint limit. In optically selected samples, the stellar masses of star forming galaxies near the survey limit are smaller than the stellar masses of galaxies near the survey limit without star formation. Thus, near infrared selection significantly reduces this potential systematic bias.

There are two related but separable issues when studying star formation rates in cluster galaxies. The first is the fraction of the total galaxy population with significant current star formation. Bright galaxies in the cores of clusters show little evidence of recent star formation; we probe the radial extent of this effect. The second issue is the distribution of star formation rates among galaxies with current star formation. Separating these issues should help clarify the physical mechanisms responsible for the transformation (Balogh et al. 2004). For instance, mechanisms which truncate star formation on short timescales (like ram pressure stripping) would likely produce a relatively sharp population gradient but leave the distribution of SFRs unchanged. Mechanisms which operate over several Gigayears would likely produce milder population gradients but with a larger change in the SFR distribution (i.e., dense regions would contain more galaxies with small but non-zero SFRs).

We describe the observations in §2. We discuss the distribution of galaxies with and without H $\alpha$  emission in §3. In §4, we discuss the distribution of equivalent widths in different environments. We discuss our results in §5 and conclude in §6. We assume a cosmology of  $H_0 = 100 h \text{ km s}^{-1}$ ,  $\Omega_m = 0.3$ ,  $\Omega_\Lambda = 0.7$  throughout.

## 2. OBSERVATIONS

### 2.1. The CAIRNS Cluster Sample

We selected the CAIRNS parent sample from all nearby ( $cz < 15,000 \text{ km s}^{-1}$ ), Abell richness class  $R \geq 1$  (Abell et al. 1989), X-ray luminous ( $L_X > 2.5 \times 10^{43} h^{-2} \text{ erg s}^{-1}$ ) galaxy clusters with declination  $\delta > -15^\circ$ . Using X-ray data from the X-ray Brightest Abell Clusters catalog (Ebeling et al. 1996), the parent cluster sample contains 14 systems. We selected a representative sample of 8 of these 14 clusters (Table 1). The cluster properties listed in Table 1 are from Paper I. The 6 clusters meeting the selection criteria but not targeted in CAIRNS are: A193, A426, A2063, A2107, A2147, and A2657. The 8 CAIRNS clusters span a variety of morphologies, from isolated clusters (A496, A2199) to major mergers (A168, A1367). Note that we omit A576 from the present sample because it lacks uniform, homogeneous spectroscopy (§2.3).

The redshift limit is set by the small aperture of the 1.5-m Tillinghast telescope used for the vast majority of our spectroscopic observations. The richness minimum guarantees that the systems contain sufficiently large numbers of galaxies to sample the velocity distribution. The X-ray luminosity minimum guarantees that the systems are real clusters and not superpositions of galaxy groups (cf. the discussion of A2197 in Rines et al. 2001a, 2002). Three additional clusters with smaller X-ray luminosities (A147, A194 and A2197) serendipitously lie in the survey regions of A168 and A2199. A147 and A2197 lie at nearly identical redshifts to A168 and A2199; their dynamics are probably dominated by the more massive cluster (Rines et al. 2002). A194, however, is cleanly separated from A168 and we therefore analyze it as a ninth system. The inclusion of A194 extends the parameter space covered by the CAIRNS sample. The X-ray temperature of A194 listed in Ebeling et al. (1996) is an extrapolation of the  $L_X - T_X$  relation; in Table 1 we therefore list the direct temperature estimate of Fukazawa et al. (1998) from *ASCA* data. Fukazawa et al. (1998) list X-ray temperatures for 6 of the 9 CAIRNS clusters which agree with those listed in Ebeling et al. (1996).

In Paper I, we applied a hierarchical clustering analysis (described in Diaferio 1999) to the redshift catalogs to determine the central coordinates and redshift of the largest system of galaxies in each cluster. We adopt these hierarchical centers as the cluster centers. We then used the caustic technique to compute mass profiles for the clusters to very large radii. We define the cluster virial region as the volume inside  $r_{200}$  ( $r_\delta$  is the radius within which the enclosed mass density is  $\delta\rho_c$ , where  $\rho_c$  is the critical density). The infall region is the volume between  $r_{200}$  and  $r_{3.5}$ , which corresponds to the turnaround radius  $r_t$  of a spherical overdensity (Regös & Geller 1989). Empirically,  $r_t \approx 5r_{200}$ . Note that  $R_\delta$  refers to  $r_\delta$  in projection; it has the same numerical value and is used only to emphasize projected quantities.

### 2.2. 2MASS Photometry

2MASS is an all-sky survey with uniform, complete photometry (Nikolaev et al. 2000) in three infrared bands (J, H, and  $K_s$ , a modified version of the K filter truncated at longer wavelengths). We use photometry from the final extended source catalog (XSC, Jarrett et al. 2000). The 2MASS XSC computes magnitudes in the  $K_s$ -band using several different methods, including aperture magnitudes

TABLE 1  
CAIRNS PARENT POPULATION

Cluster	X-ray Coordinates		$cz_{\odot}$ km s $^{-1}$	$\sigma_p$ km s $^{-1}$	$L_X$ $10^{43} h^{-2}$ ergs s $^{-1}$	$T_X$ keV	Richness
	RA (J2000)	DEC (J2000)					
A119	00 56 12.9	-01 14 06	13268	$698^{+36}_{-31}$	8.1	5.1	1
A168	01 15 08.8	+00 21 14	13395	$579^{+36}_{-30}$	2.7	2.6	2
A496	04 33 35.2	-13 14 45	9900	$721^{+35}_{-30}$	8.9	4.7	1
A539	05 16 32.1	+06 26 31	8717	$734^{+53}_{-44}$	2.7	3.0	1
A576 <sup>a</sup>	07 21 31.6	+55 45 50	11510	$1009^{+41}_{-36}$	3.5	3.7	1
A1367	11 44 36.2	+19 46 19	6495	$782^{+56}_{-46}$	4.1	3.5	2
Coma	12 59 31.9	+27 54 10	6973	$1042^{+33}_{-30}$	18.0	8.0	2
A2199	16 28 39.5	+39 33 00	9101	$796^{+38}_{-33}$	9.1	4.7	2
A194	01 25 50.4	-01 21 54	5341	$495^{+41}_{-33}$	0.4	2.6	0

<sup>a</sup>Omitted from the present sample because it lacks uniform spectroscopy.

(using a circular aperture with radius 7''), isophotal magnitudes which include light within the elliptical isophote corresponding to  $\mu_{K_s}=20$  mag/arcsec $^2$ , Kron magnitudes, and extrapolated “total” magnitudes (Jarrett et al. 2000). The sky coverage of the catalog is complete except for small regions around bright stars.

The 2MASS isophotal magnitudes omit  $\sim 15\%$  of the total flux of individual galaxies (K01). C01 compare 2MASS photometry from the Second Incremental Data Release (2IDR) with deeper infrared photometry from Loveday (2000). They find that Kron magnitudes are slightly fainter than the total magnitudes in deeper surveys (see also Andreon 2002) and that 2MASS extrapolated total magnitudes are slightly brighter than Kron magnitudes (for the deeper survey these are close to total magnitudes) from the deeper survey. 2MASS is a relatively shallow survey and thus likely misses many low surface brightness galaxies (Andreon 2002; Bell et al. 2003). In this work we focus on bright galaxies (which typically have high surface brightness); thus, this bias is less important here than for estimates of the global luminosity density or stellar mass density. Except where noted, we define “bright galaxies” as those with  $M_{K_s} = -22.7 + 5\log h$ .

We use the  $K_s$ -band survey extrapolated “total” magnitudes. Galactic extinction is minor in the near-infrared. We correct for Galactic extinction by using the value in the center of the cluster which we estimate from the dust maps of Schlegel et al. (1998). We make K corrections and evolutionary corrections of  $<0.15$  magnitudes based on Poggianti (1997). Because these corrections are small and not strongly dependent on the galaxy model at the redshifts of the CAIRNS clusters, we apply a uniform correction for all galaxies in a given cluster interpolated from the model Elliptical SED with solar metallicity and a star-formation e-folding time of 1 Gyr.

### 2.3. Spectroscopy

We have collected 15767 redshifts within a radius of  $\sim 10h^{-1}$  Mpc of the 9 clusters in the CAIRNS sample (Paper I) and an additional 515 redshifts to obtain complete near-infrared selected samples (Rines et al. 2004). The spectra were obtained with the FAST spectrograph (Fab-

ricant et al. 1998) on the 1.5-m Tillinghast telescope of the Fred Lawrence Whipple Observatory (FLWO). FAST is a high throughput, long slit spectrograph with a thinned, backside illuminated, antireflection coated CCD detector. The slit length is 180''; our observations used a slit width of 3'' and a 300 lines mm $^{-1}$  grating. The slit orientation is fixed at 90° (E-W) for nearly all observations to maximize observing efficiency. This setup yields spectral resolution of 6-8 Å and covers the wavelength range 3600-7200 Å. We obtain redshifts by cross-correlation with spectral templates of emission-dominated and absorption-dominated galaxy spectra created from FAST observations (Kurtz & Mink 1998). The typical systematic uncertainty in the redshifts is 30 km s $^{-1}$ ; the statistical uncertainty is usually comparable.

The target catalogs were constructed first with photographic plates (see details in Paper I) and later with 2MASS (Rines et al. 2004). The redshift catalogs are essentially complete to at least  $M_{K_s} = -22.7 + 5\log h$  (our definition of “bright galaxies”) with some sampling of fainter galaxies from the optical catalogs. This limit is roughly 1 magnitude fainter than  $M_{K_s}^*$  for field galaxies (Cole et al. 2001) and contains  $\sim 60\%$  of the total cluster light (in galaxies) assuming that the cluster and field LFs are identical. The completeness limits in absolute magnitudes of the clusters lie in the range  $-22.70 \leq M_{K_s, \text{lim}} - 5\log h \leq -21.42$ ; we use these slightly deeper limits to reduce statistical uncertainties when studying individual cluster properties with small numbers of “bright galaxies”. We drop A576 from the sample because most of the spectra in the cluster core were obtained with different instrumentation (Mohr et al. 1996). Rather than correct for differences in instrumentation for this one cluster, we restrict our study to clusters with substantially complete FAST spectroscopy. Table 2 lists the number of bright galaxies in the virial region of each cluster ( $R_p \leq R_{200}$ ), in the infall region ( $1 < R_p/R_{200} \leq 5$ ), and the sum of the two. The radius  $r_{200}$  is the radius within which the enclosed matter density is 200 times the critical value ( $R_{200}$  is this radius for projected radii). In a critical density universe,  $r_{200}$  is about equal to the virial radius; in a  $\Lambda$ CDM universe, the virial radius is approximately  $r_{100} \approx 1.4r_{200}$ . Table

2 shows that we have FAST spectra for 92.4% of bright galaxies with  $R_p/R_{200} \leq 5$ . Note that A119 and A168 have a projected separation of  $10.7 h^{-1}\text{Mpc} \approx 9.7R_{200}$ . Thus, the outskirts of A119 and A168 overlap.

An important difference between the FAST spectra collected for CAIRNS and those collected for other, larger redshift surveys (Colless et al. 2001; Stoughton et al. 2002) is that the S/N is similar for bright and faint galaxies. CAIRNS suffers no incompleteness due to fiber placement constraints. Another difference is that the long-slit FAST spectra sample light from larger fractions of the galaxies than fiber spectra. Thus, the effects of aperture bias (e.g., Kochanek et al. 2003; Kewley et al. 2005) on spectral classification are greatly reduced. Carter et al. (2001) show that a spectroscopic survey of field galaxies obtained with identical instrumentation in a similar redshift range contains no significant aperture bias.

However, there is an important caveat about aperture bias. Many Virgo spirals (Koopmann & Kenney 2004) as well as some spirals in other nearby clusters (Vogt et al. 2004) show evidence of truncated  $H\alpha$  disks. Because these truncated disks are rare in samples of field galaxies, estimates of aperture bias based on field samples (Carter et al. 2001; Kewley et al. 2005) may not apply to cluster samples. We discuss this issue further in §5. The CAIRNS spectra should present an unbiased picture of the star formation properties of the inner parts of galaxies (radii  $\lesssim 3$  kpc), but future studies (with either narrowband imaging and/or integrated spectra) are required to see whether these relations accurately represent global star formation properties.

Our spectroscopic catalog contains many foreground and background galaxies. We can use these spectra to investigate possible systematic differences between galaxies in cluster, infall, and field environments. Note, however, that our catalog of field galaxy spectra is not complete. In particular, we do not have spectra for (preferentially bright) galaxies with previously measured redshifts which we classify as foreground or background galaxies. We use field galaxy spectra only in the redshift interval 2000–12000  $\text{km s}^{-1}$  to minimize the effects of aperture corrections and to avoid Virgocentric infall (Table 2). Curiously, the distribution of absolute magnitudes  $M_{K_s}$  for our field galaxies with FAST spectra is extremely similar to that of cluster/infall members (a K-S test fails to differentiate them at the 90% confidence level despite having samples of over 600 galaxies), while both differ significantly from the distribution of galaxies without FAST spectra. This happy circumstance means that our field sample is well matched to our cluster and infall region sample.

#### 2.4. Spectroscopic Indices and Types

We measure spectroscopic properties of the galaxies in several emission lines. We extract 1D spectra from the 2D spectra selecting apertures along the slit which maximize the S/N. The resulting 1D spectra thus oversample the inner few kpc of the galaxies relative to integrated spectra. We calculate equivalent widths in the lines from the 1D spectra using the bandpasses for lines and continua listed in Table 3. These bandpasses are the ones used by Carter et al. (2001) to study galaxies in the 15R survey except for  $H\beta$ , for which we modify the continuum region

so that it excludes the  $[\text{OIII}]\lambda 4949$  line. Because we focus on emission lines, we adopt the convention that emission lines have positive equivalent width.

We divide the sample into two main subsamples of galaxies with and without emission lines (we refer to the latter sample as absorption galaxies). We define the emission line sample as galaxies with  $\text{EW}[H\alpha] \geq 2.0\text{\AA}$ . We do not correct for stellar absorption, which is typically  $\approx 1.0\text{\AA}$  (Balogh et al. 2004). We also do not correct  $\text{EW}[H\alpha]$  for absorption by dust because we assume that the extinction to continuum and to HII regions are identical. If this assumption is incorrect (Calzetti 2001), then Balmer decrements are necessary to obtain accurate SFR estimates. However, the environmental trends we investigate here should be robust to this effect unless the relative extinctions of continuum and HII regions depend on environment. The median statistical uncertainty in  $\text{EW}[H\alpha]$  is  $\approx 0.3\text{\AA}$ ; the spectral classification of emission/non-emission lines is robust (less than 3% of galaxies have  $\text{EW}[H\alpha]$  within  $1\sigma$  of  $2.0\text{\AA}$ ). Our cut-off for emission line galaxies is slightly more generous than that of Balogh et al. (2004), who uses  $\text{EW}[H\alpha] \geq 4\text{\AA}$  (after adding  $1.0\text{\AA}$  to the EW to correct roughly for  $H\alpha$  absorption). We do not convert  $\text{EW}[H\alpha]$  to fluxes because few of the spectra have significant detections of  $H\beta$  required to estimate the extinction correction. The single criterion  $\text{EW}[H\alpha] \geq 2\text{\AA}$  leads to some contamination of the absorption galaxy subsample by galaxies with obscured star formation and/or obscured AGN. For this reason and because the signal-to-noise ratios of the spectra are not uniform across the sample, this definition may misclassify galaxies with weak emission lines in their spectra as absorption line galaxies. The classification is therefore a separation of gas-rich (including AGN) and gas-poor systems, with some contamination of the gas-poor subsample.

We directly compare several FAST spectra in the fields of A119 and A168 to SDSS spectra and find that there is very good agreement in spectral classification (the presence or absence of  $H\alpha$  emission). There is substantial, but not surprising, scatter in the values of  $\text{EW}[H\alpha]$ , probably due to the inhomogeneous nature of  $H\alpha$  emission (e.g., the inclusion or exclusion of a single HII region can significantly affect the inferred  $\text{EW}[H\alpha]$ ). A full comparison of FAST and SDSS spectra is beyond the scope of this work.

We further divide the subsample of galaxies with emission lines into AGN-dominated galaxies and star forming galaxies using the line diagnostics of Kewley et al. (2001). The lack of accurate  $H\beta$  data (due to stellar absorption and weaker emission lines) prevents this classification from being very robust; thus we inspect all the emission-line spectra interactively with the IRAF routine *splot* to include AGN with no detected  $H\beta$  or where broad lines affect the line indices. These diagnostics only classify emission as dominated by AGN if it is impossible to reproduce the emission lines with HII region photoionization models. The diagnostics of Kewley et al. (2001) classify some galaxies as star forming that would be classified by Veilleux & Osterbrock (1987) as AGN. The AGN fraction is small among bright  $K_s$ -selected galaxies; within  $5R_{200}$ , the AGN fraction is  $2.8 \pm 0.6\%$ . This fraction is smaller than the  $\sim 20\%$  in the studies of Carter et al. (2001) and Kauffmann et al. (2003), mostly due to the different diagnostics used. The AGN fraction is sufficiently small that we ig-

TABLE 2  
CAIRNS VIRIAL AND INFALL REGION MEMBERSHIP

Cluster	$N_{200}$	$N_{inf}$	$N_{tot}$
A119	52(40)	71(67)	123(107)
A168	38(25)	79(74)	117(99)
A496	40(38)	40(37)	80(77)
A539	32(21)	26(22)	58(43)
A1367	44(44)	58(57)	102(101)
Coma	97(97)	115(115)	212(212)
A2199	55(50)	159(145)	214(195)
A194	20(20)	20(20)	40(40)
All	378(335)	568(539)	946(874)
Field			656

<sup>a</sup>Numbers in parentheses are the number of galaxies with FAST spectra.

TABLE 3  
LINE INDEX DEFINITIONS

Index	Blue Continuum ( $\text{\AA}$ )	Line Region ( $\text{\AA}$ )	Red Continuum ( $\text{\AA}$ )
[OII]	3727.3 $\text{\AA}$	3716.3—3738.3	3738.3—3803.0
H $\beta$	4861.3 $\text{\AA}$	4841.3—4881.3	4891.3—4951.3
[OIII]	5006.8 $\text{\AA}$	4995—5019	5021—5087
[NII]	6548.1 $\text{\AA}$	6538.1—6558.1	6597—6627
H $\alpha$	6562.8 $\text{\AA}$	6554.5—6574.5	6597—6627
[NII]	6583.4 $\text{\AA}$	6573.4—6593.4	6597—6627

nore the AGN/HII classification in the next section where we discuss the environmental dependence of the fraction of galaxies with emission lines.

### 3. DISTRIBUTION OF SPECTROSCOPIC TYPES

#### 3.1. Radial Distribution of Spectroscopic Types

Figure 1 shows the fraction of galaxies (with FAST spectra) in the emission/absorption subsample as a function of clustrocentric radius. The solid lines in each panel show the expected fraction of emission line galaxies in a field sample with the same limiting absolute magnitude as the cluster in that panel. We estimate this fraction from the field galaxy spectra in our catalog in the redshift interval  $2000\text{--}12000\text{ km s}^{-1}$ . The fraction of bright ( $M_{K_s} \leq -22.7 + 5\log h$ ) galaxies with emission lines is similar to the fraction in the complete magnitude-limited survey of Carter et al. (2001). The limiting absolute magnitudes of the clusters lie in the range  $-22.70 \leq M_{K_s,lim} - 5\log h \leq -21.42$ ; the fractions of emission line galaxies in similarly selected “field” samples lie in the range  $0.27 \leq f_{ELG} \leq 0.46$ , similar to the fraction in the complete magnitude-limited survey of Carter et al. (2001). Figure 1 and a similar figure in §3.5 are the only results shown for a cluster-dependent  $M_{K_s,lim}$  rather than for only “bright galaxies” (defined by  $M_{K_s} \leq -22.7 + 5\log h$ ). The emission fraction profiles to a fixed luminosity cutoff are very similar but have poorer statistics, especially for the poor cluster A194. The outskirts of A119 and A168 overlap (§2.3); Figure 1 shows that the emission-line fraction at the midpoint is roughly equal to the field value.

We confirm that the fraction of galaxies with current star formation does not reach the field value until  $2\text{--}3 R_{200}$  ( $R_{200}$  roughly equals the virial radius) from the centers of clusters (Abraham et al. 1996; Balogh et al. 1997; Diaferio et al. 2001; Ellingson et al. 2001; Lewis et al. 2002; Gómez et al. 2003; Balogh et al. 2004). Figure 1 demonstrates that this effect is observable in individual clusters, although there appear to be cluster-to-cluster variations in the exact shape of this profile. As in Paper I, clusters are ordered left to right and top to bottom in order of decreasing X-ray temperature, a good proxy for virial mass. The gradients appear smoothest for the hottest clusters, although the coolest cluster (A194) also shows a smooth gradient. Figure 2 shows the emission fraction in the composite CAIRNS cluster; the emission fraction converges to the field value at  $\approx 2R_{200}$ . Because the cluster masses are well determined (the statistical uncertainties in the corrected virial masses are  $\lesssim 15\%$ ; see Paper I), the uncertainties in  $r_{200} \propto M^{1/3}$  should not affect the cluster-to-cluster comparison or the construction of the composite cluster. Assuming that the population variation is caused by environment, this result can be interpreted in two ways. Either (1) infalling galaxies are “preprocessed” at high densities in filaments and groups in the infall regions, or (2) a significant number of galaxies projected at large radii have already passed near the cluster center and are observed on “first outfall” or second infall. The “preprocessing” interpretation implicates relatively local processes such as galaxy-galaxy interactions; the latter “backsplash” scenario implicates processes such as ram pressure stripping that are strongest near cluster centers.

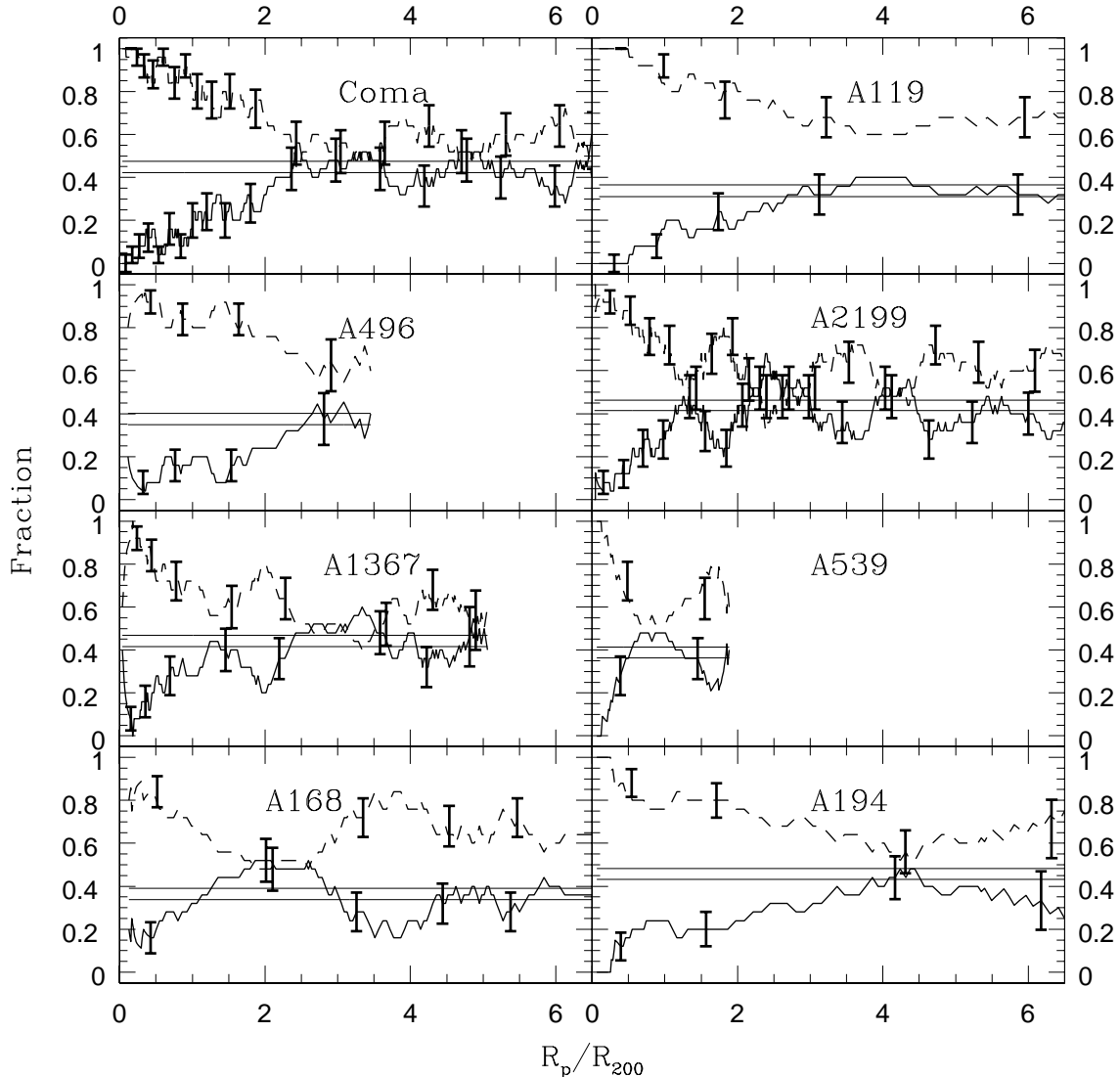


FIG. 1.— Fraction of bright galaxies with (solid lines) and without (dashed lines)  $H\alpha$  emission as a function of distance from the cluster center in units of  $R_{200}$ . The lines show the fractions in moving averages of 25 galaxies and the errorbars are placed at independent bins and indicate Poisson uncertainties. The samples for each cluster are selected by absolute magnitude ( $M_{K_s} \leq M_{K_s,lim}$ ) with a slightly different limit for each cluster. Horizontal lines in each panel show the  $1\text{-}\sigma$  range of the fraction of emission line galaxies in field samples to the same limiting luminosity.

The infall region of A2199 offers an interesting discriminant between the two scenarios because it contains several X-ray emitting groups (Rines et al. 2001b, 2002). Under the preprocessing scenario we would expect that the fraction of galaxies with emission lines would not converge to the field value until well outside  $r_{200}$ . The fraction of emission-line galaxies in A2199 quickly rises to the field value just outside  $R_{200}$ , but the fraction then *decreases* at the radius of the infalling X-ray groups A2197W and A2197E (Figure 1). This result supports the preprocessing scenario.

Unlike the other clusters, the emission fraction in A168 shows only a very weak radial trend. Part of this difference results from the unrelaxed nature of A168 (Paper I); the X-ray and optical centers are offset by  $160 h^{-1}\text{kpc}$ . When we plot the emission fraction versus distance from the X-ray center, the trend is closer to those of the other CAIRNS

clusters. Although these cluster-to-cluster variations are interesting, we caution the reader that the appearance of clusters can vary dramatically depending on projection effects (e.g., Diaferio 1999); thus one must be cautious not to overinterpret these variations.

Figure 3 shows the number density profiles of emission and absorption galaxies. Because the caustics which we use to define membership extend to a different radius  $R_{max}$  for each cluster (Paper I), the profiles are incompletely sampled (and therefore underestimated) outside  $\sim 2R_{200}$ . We do not weight by cluster richness; each galaxy has an equal weight. Both profiles are fit well by NFW profiles (Navarro et al. 1997), with scale radii of  $\approx 0.23r_{200}$  for the absorption galaxies and  $\approx 1.25r_{200}$  for the emission-line galaxies. The implied NFW concentration parameter  $c = r_{200}/r_s$  is therefore 4.3 (3.3-5.9 at 68% confidence) and 0.8 (0.4-1.7 at 68% confidence) for absorption and emis-

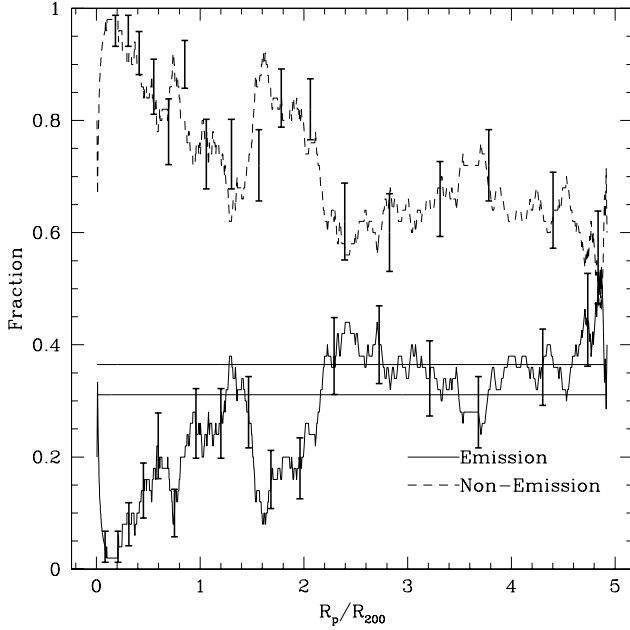


FIG. 2.— Fraction of bright galaxies ( $M_{K_s} \leq -22.7$ ) with (solid lines) and without (dashed lines) H $\alpha$  emission as a function of distance from the composite cluster center in units of  $R_{200}$ . The lines show the fractions in moving averages of 50 galaxies and the error-bars are placed at independent bins and indicate Poisson uncertainties. Horizontal lines show the 1- $\sigma$  range of the fraction of emission line galaxies in field samples to the same limiting luminosity.

sion line galaxies respectively, and  $c \approx 3.3$  for all galaxies combined. This last number agrees with the results of a separate study which uses statistical background subtraction to determine membership (Lin et al. 2004). For comparison, the caustic mass profiles yield estimates of  $c = 5 - 17$  for the CAIRNS clusters. Cluster galaxies are therefore less concentrated than dark matter in the cluster, although the concentration of absorption-line galaxies is similar to the smallest values of  $c$  of the mass profiles.

Carlberg et al. (1997) fit Hernquist (1990) profiles to the number density profiles of blue and red samples from the CNOC1 survey. Using Hernquist profiles, the scale radius of the absorption-line galaxy sample in CAIRNS ( $1.13 \pm 0.18$ ) exceeds the scale radius ( $0.56 \pm 0.10$ ) of red galaxies in the CNOC1 survey Carlberg et al. (1997), and the scale radius of the emission line galaxies ( $3.2^{+2.1}_{-1.2}$ ) exceeds that of the blue galaxies in CNOC1 ( $1.82 \pm 0.27$ ). This comparison suggests that emission-line galaxies are a subsample of blue galaxies with a more extended distribution and that absorption-line galaxies are a combination of red and blue galaxies. Indeed, 30% of CNOC1 cluster galaxies are classified as blue; only 10% of CAIRNS cluster galaxies inside  $R_{200}$  are emission-line galaxies. The different scale radii may reflect the fact that CNOC1 includes few galaxies outside  $R_{200}$ .

Assuming that the NFW profiles accurately represent the true profiles, we can estimate the number of “infall interlopers,” galaxies with  $R_p \leq R_{200}$  but  $r_{3D} > r_{200}$ . At least 20% of absorption line galaxies and 50% of emission line galaxies are infall interlopers. Figure 4 shows the fraction of galaxies projected within  $R_p$  with physical radii  $r_{3D} > R_p$ . The fraction of infall interlopers increases

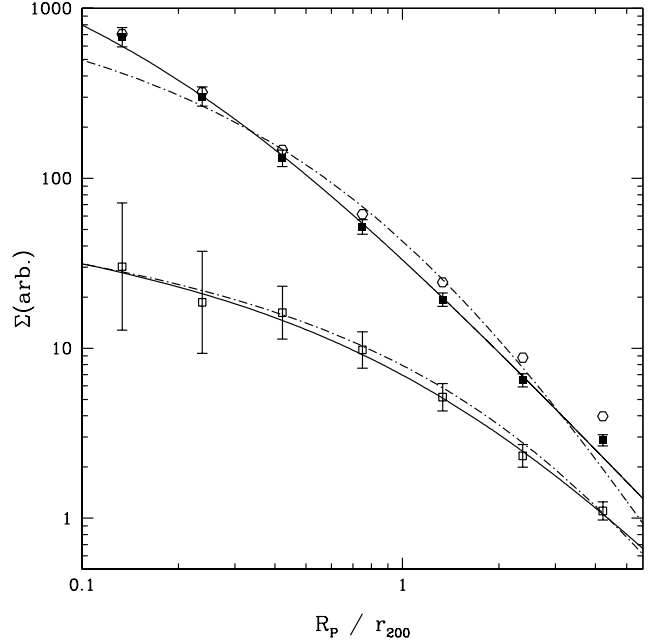


FIG. 3.— Surface number density profiles of bright galaxies with (open squares) and without (filled squares) H $\alpha$  emission in units of  $R_{200}$  (open hexagons show the sum). The solid (dash-dotted) lines show the best-fit NFW and (Hernquist) profiles.

dramatically as the projected radius  $R_p$  decreases. This result is consistent with the simulations of Diaferio et al. (2001), who show the fraction of galaxies with  $r_{3D} > r_{200}$  as a function of  $R_p$  (see their Figure 13). The actual fraction of infall interlopers probably varies significantly from cluster to cluster due to the non-uniform distribution of galaxies in the infall region (i.e., groups and filaments). This result validates an assumption often used in cluster studies, namely, that star-forming/blue/spiral galaxies are not good tracers of the mass distribution in the virial region (e.g., Carlberg et al. 1997). It is interesting to note that even among absorption-line galaxies, the fraction of infall interlopers is 20%. Because the density of the infall region increases with redshift (Ellingson et al. 2001), the fraction of infall interlopers probably increases with redshift.

Projection effects have important implications for the analysis of cluster galaxies. The strong radial dependence of the fraction of galaxies with emission lines suggests that many and perhaps all emission-line galaxies projected inside  $r_{200}$  actually lie at larger radii. These galaxies may lie in the infall region or they may be interlopers from the field. The “infall interlopers” alone comprise at least 50% of emission-line galaxies with  $R_p \leq r_{200}$ .

Among bright galaxies, the fraction of galaxies without emission lines is still quite large well outside  $R_{200}$ . This result shows that some early-type galaxies projected inside  $R_{200}$  lie at greater radii and thus that their kinematics might not represent a relaxed population. Restricting virial mass estimates to galaxies without emission lines is effective at removing the emission-dominated “infall interlopers” (galaxies inside  $r_t$  but outside  $r_{200}$ ) but does not remove the infall interlopers without emission lines.

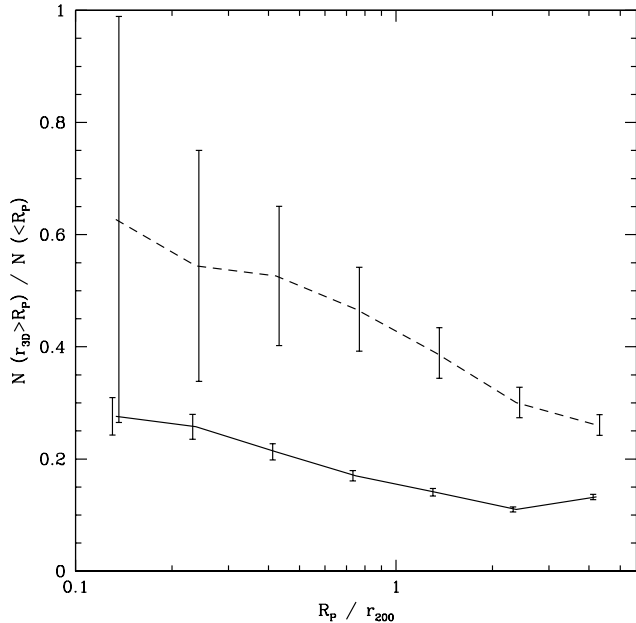


FIG. 4.— Fraction of galaxies within projected radius  $R_p$  that are “infall interlopers” (galaxies within the cluster virial or infall region but with physical radii  $r_{3D} > R_p$ ) versus  $R_p$ , computed assuming NFW number density profiles for both populations (Figure 3). The errorbars show the Poissonian uncertainties on the number density profiles and do not include any uncertainty in the model. Dashed and solid lines represent emission and absorption galaxies respectively.

### 3.2. Kinematic Distribution of Spectroscopic Types

Figure 5 shows the velocity distribution of emission- and absorption-line galaxies projected inside  $R_{200}$ . We find no evidence for kinematic segregation; a two-sample K-S test indicates a 28% probability that two samples drawn from the same parent distribution would show a larger difference. We do find a larger velocity dispersion for the emission-line galaxies with an F test, but this test assumes that the parent distributions are Gaussian. Bright emission-line galaxies are quite rare in clusters; even after stacking the nine CAIRNS clusters, there are 42 bright emission-line galaxies inside  $R_{200}$ , compared to 293 bright absorption-line galaxies (43 bright galaxies have no FAST spectra).

Figure 6 shows the velocity dispersion profiles (VDPs) of emission and absorption line galaxies. The profiles are quite similar. We obtain similar results when including all galaxies brighter than  $M_{K_s} = -21.0$  (an incomplete sample), suggesting that the similarity of the VDPs extends to fainter magnitudes. There is also no significant difference between the velocity distributions in the interval  $1 < R_p/R_{200} \leq 2$  (bottom panel of Figure 5). Figure 7 shows redshift versus projected radius for the CAIRNS member galaxies with different symbols for emission and absorption line galaxies.

These results contradict conventional wisdom about the velocity distribution of early and late-type galaxies. Early studies of kinematic differences in Virgo (Huchra 1985; Binggeli et al. 1987) show different velocity dispersions for early and late-type galaxies, but Virgo is a very complex

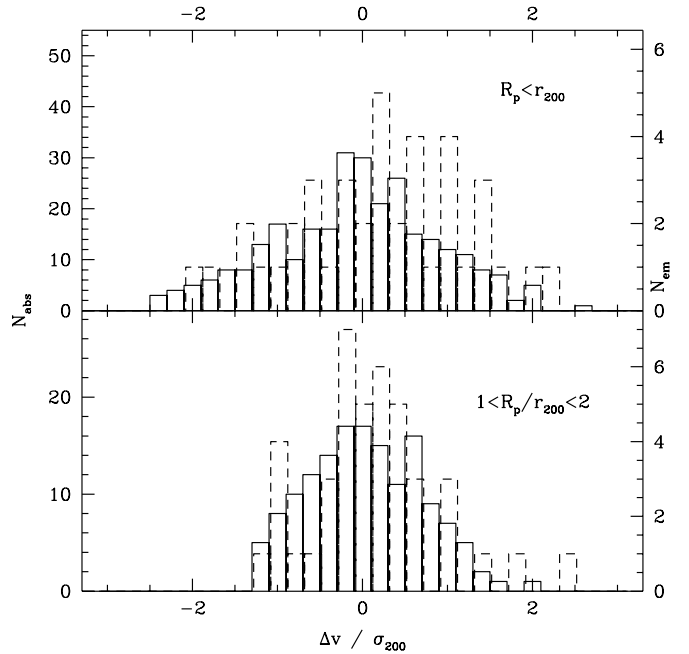


FIG. 5.— (Top panel) Velocity distribution of galaxies projected inside  $R_{200}$  with (dashed line) and without (solid line)  $H\alpha$  emission. (Bottom panel) Same as top panel for galaxies projected in the interval  $1 < R_p/r_{200} \leq 2$ . Backsplash galaxies should be peaked at zero velocity.

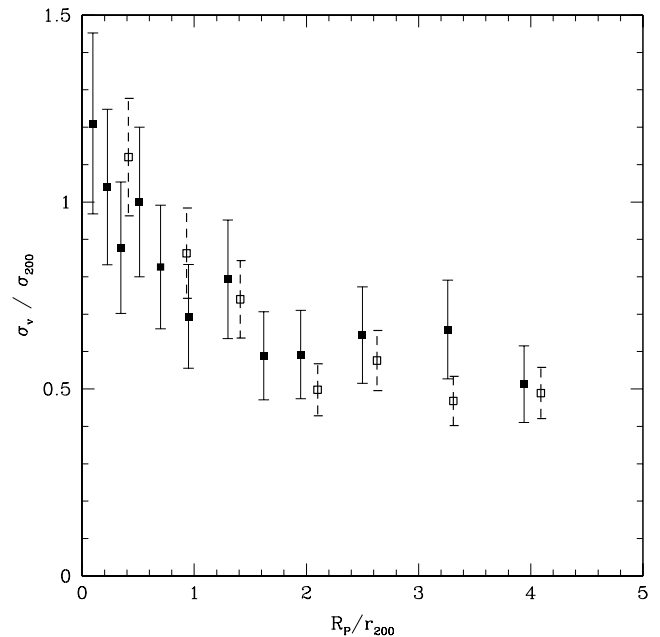


FIG. 6.— Velocity dispersion profiles of bright galaxies with (dashed line) and without (solid line)  $H\alpha$  emission.

system and neither investigation uses a nonparametric K-S test. Similar differences exist in A576 for emission- and absorption-dominated galaxies (Mohr et al. 1996), and for red and blue galaxies projected in the virial regions of clusters (Kent & Gunn 1982; Colless & Dunn 1996; Carlberg et al. 1997). Mohr et al. (1996) found that the velocity dispersions differ according to an F test, but “a K-S test



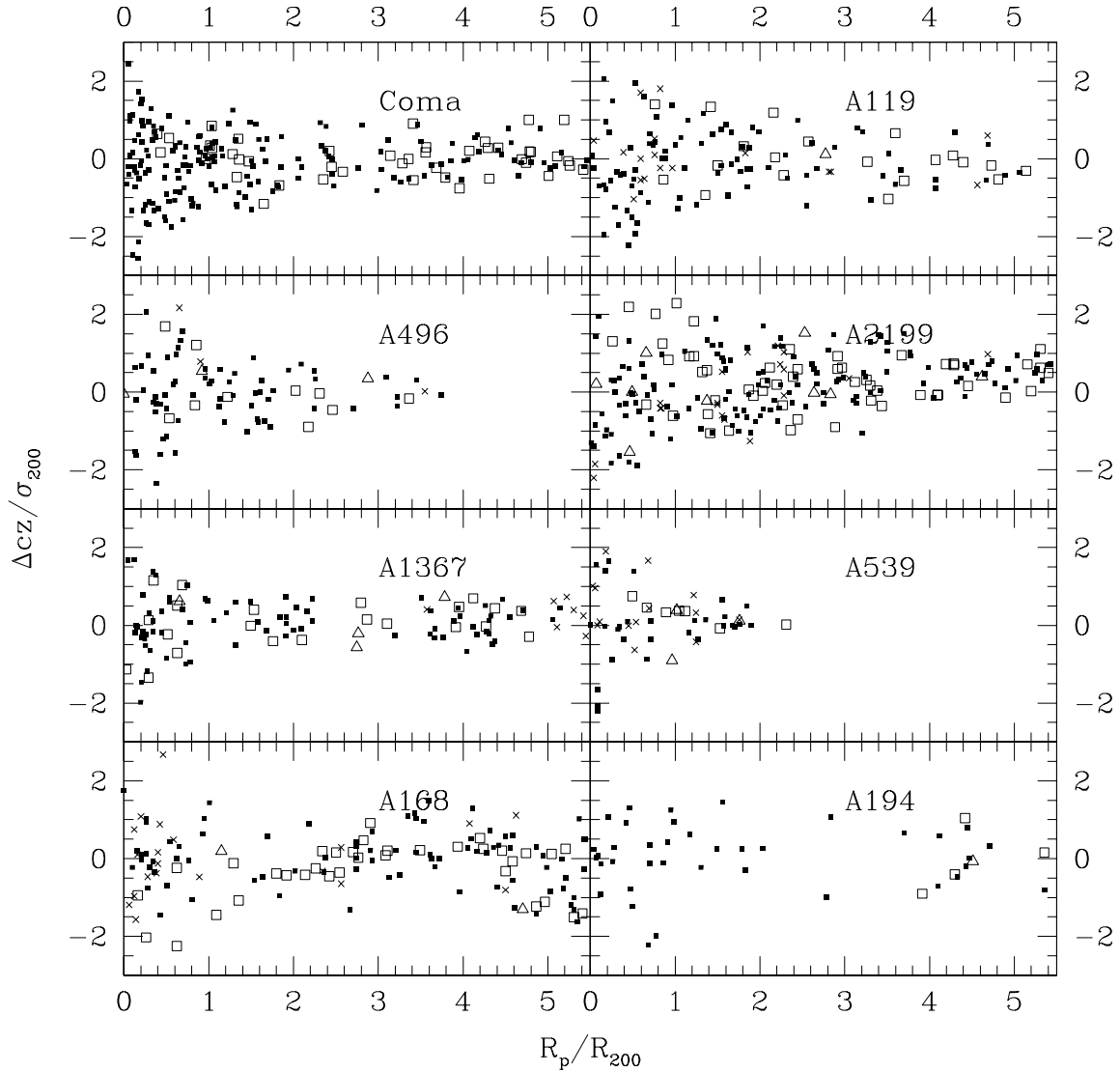


FIG. 7.— Velocity versus projected radius for bright galaxies with (open squares and triangles) and without (dots) H $\alpha$  emission (crosses are galaxies without FAST spectra). Squares and triangles indicate HII and AGN type emission respectively.

fails to distinguish between the two velocity distributions.” In the CNOC1 clusters, red and blue galaxies have significantly different VDPs, but Jeans’ analysis yields consistent cluster masses for both red and blue populations (Carlberg et al. 1997). The CNOC1 results therefore suggest that the blue galaxy population is in dynamical equilibrium with the same underlying mass profile as the red galaxies. A galaxy population on first infall is not expected to be in equilibrium with the underlying mass profile and would not necessarily satisfy the Jeans’ equations. The emission-line galaxies in CAIRNS have the same velocity distribution but a different spatial distribution than the absorption-dominated galaxies; the CAIRNS emission-line galaxies are therefore not in dynamical equilibrium with the mass profile traced by the absorption-dominated galaxies.

To test the robustness of previous results, we revisit the analysis of Colless & Dunn (1996), who found a difference between red and blue galaxies at the 99.2% confidence level

with a K-S test in the Coma cluster. They use the photometric catalog of Godwin et al. (1983) based on photographic plates to identify galaxies within and blueward of a color-magnitude relation (see their Figure 12). We reproduce their color cut using an updated redshift catalog from NED and Paper I. Using a similar membership criterion ( $4000 \leq cz \leq 10000 \text{ km s}^{-1}$ ), we find that the difference is only significant at 97.5%; the significance drops to 90.0% with the redshift cut  $4000 \leq cz \leq 9000 \text{ km s}^{-1}$ . Their result is based only on galaxies classified in the larger of two subclusters defined by the KMM algorithm; we perform a similar cut by selecting only galaxies within  $30'$  of the center of Coma, but obtain nearly identical results (97.6% versus 97.5%). We therefore conclude that the kinematic difference between blue and red galaxies claimed by Colless & Dunn (1996) is not robust.

The inclusion of galaxies at the edges of the distributions risks including interlopers from the field; because field galaxies have a much larger fraction of blue galaxies,

these interlopers are likely to be blue galaxies. Inclusion of these field interlopers artificially increases the velocity dispersion of blue galaxies. Our membership selection from the caustics is generally more conservative than techniques such as  $3\text{-}\sigma$  clipping, which are used for sparser galaxy samples. If there are real differences in the kinematics of red and blue galaxies, these should be present in the main part of the distribution and not just in the high-velocity tails. Thus, stricter membership criteria should not mask real kinematic differences. However, looser criteria may include interlopers and artificially increase the velocity dispersion of blue galaxies relative to red galaxies.

Biviano et al. (2002) performed a more robust investigation of luminosity and morphological segregation in the ENACS clusters. They find significant differences in the  $(R, v)$  distributions of three classes of galaxy types (E+E/S0+S0, early-type spirals, and late-type spirals + emission line galaxies). However, they find no significant difference in the velocity distributions of E+E/S0+S0 and early-type spirals in the radial range  $0.25 \leq R_p/r_{200} \leq 0.75$  or in the three types in the radial range  $0.75 \leq R_p/r_{200} \leq 1.5$ . Possible explanations for the differing results include the classification used (morphology versus emission lines), the sampling of fainter galaxies in ENACS (this is particularly important for later morphological types which are rare in CAIRNS), and differences in membership assignment.

The issue of kinematic segregation among galaxy types is very subtle. The results depend significantly on membership classification, survey completeness and uniformity, survey depth, morphological versus spectroscopic classification, and the definitions of cluster centers. CAIRNS uses relatively strict membership criteria which may classify galaxies at the edges of the velocity distribution as non-members. This selection tends to decrease the difference between the two populations.

### 3.3. A Test of the “Backsplash” Scenario

Recent simulations demonstrate that a significant number of galaxies observed outside cluster virial radii are “backsplash” galaxies (Balogh et al. 2000; Mamon et al. 2004), galaxies that have passed through the virial region. HI observations of galaxies in Virgo suggest that galaxies at radii as large as  $2R_{200}$  have undergone ram pressure stripping (Solanes et al. 2002; Sanchis et al. 2002; Vogt et al. 2004), a process which requires that the galaxies have encountered dense intracluster gas present only in the core of Virgo. Sanchis et al. (2004) show that these galaxies can be backsplash galaxies.

Recent simulations by Gill et al. (2005) show that the velocity distribution of backsplash galaxies is much more centrally peaked than that of infalling galaxies (see their Figure 8; they define backsplash galaxies as those which have passed within  $1.4r_{200}$ ). If all galaxies in the interval  $1.4 < R_p/R_{200} < 2.8$  are on first infall, then the observed absolute velocity  $(|cz - cz_{\text{cluster}}|)$  distribution peaks at  $\sim 400 \text{ km s}^{-1}$ . If, instead, galaxies in this interval are a mixture of backsplash and infalling galaxies, then the observed absolute velocity distribution is peaked at zero velocity. Thus, Gill et al. (2005) suggest that the observed shape of the total velocity histogram in the interval  $1.4 < R_p/R_{200} < 2.8$  can test whether backsplash galaxies

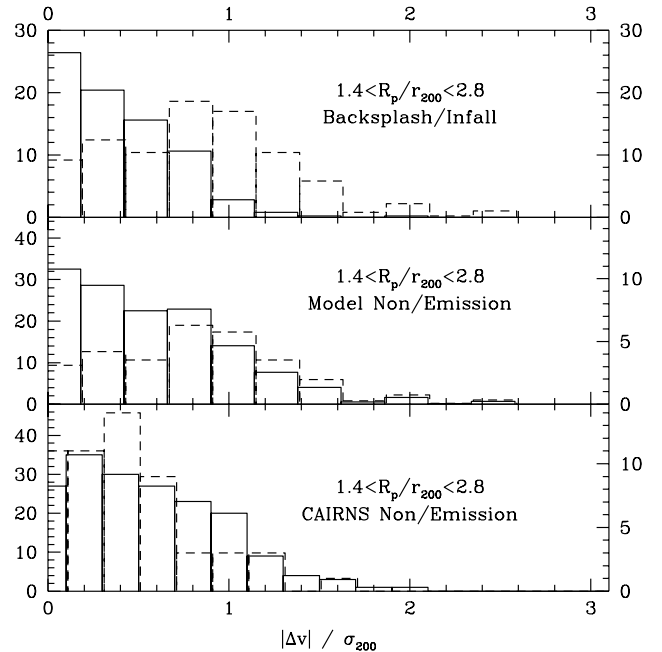


FIG. 8.— (Top panel) Velocity distribution of model cluster galaxies projected in the interval  $1.4 - 2.8R_{200}$  from the backsplash and infalling populations (solid and dashed lines respectively). (Middle panel) Velocity distribution of absorption and emission galaxies (solid and dashed lines respectively) under a toy model where all backsplash galaxies are absorption-dominated and infalling galaxies are split evenly between those with and without  $H\alpha$  emission. (Bottom panel) Observed distribution of emission/absorption galaxies (dashed/solid lines) in the CAIRNS clusters.

are present in this interval or whether all galaxies in this interval are on first infall (see their Figure 8, reproduced here as the top panel of Figure 8). We compare the total velocity distribution of CAIRNS galaxies in this radial interval with a mock total velocity distribution of backsplash plus infalling galaxies from Figure 8 of Gill et al. (2005). A K-S test fails to distinguish between the two total velocity distributions at the 95% confidence level. A K-S test clearly distinguishes between the CAIRNS total velocity distribution and both the velocity distributions of infalling and backsplash galaxies (greater than 99.9% confidence). Thus, our observations of the total velocity distribution show clear evidence for the existence of a mixed backsplash and infalling population. This result excludes extreme scenarios where all backsplash galaxies are either completely disrupted or sufficiently stripped of stars to lie below our minimum luminosity.

While the total velocity histogram provides evidence of the existence of a backsplash population, it does not contain information on the *properties* of backsplash and infalling galaxies. Gill et al. (2005) show that the velocities of backsplash galaxies are much more strongly peaked around the cluster redshift than the velocities of galaxies infalling for the first time. When projected along an observer’s line-of-sight, these differences are reduced but still significant. Thus, if the properties of a galaxy reflect whether it is backsplash or on first infall, then different galaxy distributions will have different velocity distributions. For instance, if close passage to a cluster center always truncates star formation, then a galaxy with emis-

sion lines must be on first infall and not a backsplash galaxy. We therefore propose a toy model of the back-splash scenario to convert the simulation results into observable quantities: we assume that environmental truncation of star formation in galaxies is achieved only by passage through the virial region and that the truncation mechanism is perfectly efficient.

In this toy model, the velocity distribution of emission-line (and therefore all infalling) galaxies should be skewed to larger projected velocities relative to absorption-line galaxies (which contain a mixture of backsplash and infalling galaxies) (middle panel of Figure 8). From the CAIRNS field sample,  $66 \pm 5\%$  of bright field galaxies lack emission lines, so we assume that 66% of bright galaxies on first infall will lack star formation due to non-environmental effects. The difference between the velocity distributions of the two populations should be statistically significant even if 66% of the infalling galaxies are absorption-line galaxies (a K-S test shows a difference at  $\gtrsim 99\%$  confidence for a sample the size of CAIRNS; middle panel of Figure 8). Note that Gill et al. (2005) convolve the projected velocities with a ‘typical’ observational error of  $100 \text{ km s}^{-1}$ ; because the uncertainties in our redshifts are typically  $30 \text{ km s}^{-1}$ , their Figure 8 understates the expected difference between the populations for the CAIRNS sample.

We now turn to the observations. The bottom panel of Figure 8 shows the velocity distribution of emission and absorption-line galaxies from CAIRNS in the interval  $1.4 < R_p/R_{200} < 2.8$ . While our toy model predicts significant differences, the observed velocity distributions of emission line and absorption line galaxies are indistinguishable (consistent at the 89% level with a K-S test; see the bottom panel of Figure 8).

The similarity of the velocity distributions of star-forming and passive galaxies in the interval  $1.4 < R_p/R_{200} < 2.8$  shows that this toy model of the backsplash scenario disagrees with the data. Assuming that the kinematic differences between backsplash and infalling galaxies predicted by the simulations are correct, then some emission-line galaxies must be backsplash galaxies (otherwise the velocity histogram of the emission-line galaxies in the bottom panel of Figure 8 would not be centrally peaked). That is, the observed velocity distribution of emission-line galaxies suggests that at least some of them have passed through the virial region ( $1.4r_{200}$ ) of the cluster. Thus, whether a galaxy is a backsplash galaxy or on first infall is not the primary determinant of the presence or absence of ongoing star formation (in the inner disk). The above toy model of the backsplash scenario could probably be modified to fit the data, for example by restricting the definition of back-splash galaxies to those that have passed within  $0.5r_{200}$  (rather than within  $1.4r_{200}$ ) of the central cluster or by allowing the mechanism affecting backsplash galaxies to be less than 100% efficient. It is also possible that such a passage may strip the halo gas reservoir of a galaxy that would fuel future star-formation but would not strip the existing molecular gas, allowing continued star formation for  $\sim 1$  Gyr (Larson et al. 1980) or only strip the outer disk, leading to truncated spirals (Koopmann & Kenney 2004; Vogt et al. 2004) which may not be detected in our data. We exclude only the extreme model described above.

The conclusion that a pure backsplash model does not

describe the data is consistent with the conclusion of previous investigations that the fraction of galaxies with current star formation shows the same dependence on local density both inside and outside clusters (Lewis et al. 2002; Gómez et al. 2003; Balogh et al. 2004, see §3.5). That is, both analyses suggest that mechanisms correlated with local density are more important than proximity to a cluster in determining a galaxy’s star formation rate.

Another important implication of the kinematic similarity between star-forming and passive galaxies is that the star-forming galaxies are not all interloping field galaxies; field interlopers would not show a velocity peak at the cluster redshift. Most of the emission-line galaxies in this radial bin are within the infall region. Note, however, that Figure 4 suggests that  $\sim 30\%$  of these galaxies have  $r_{3D} \gtrsim 2.8r_{200}$ .

#### 3.4. Distribution of Emission Line Galaxies on the Sky

If emission line galaxies are interlopers from the field, then their distribution on the sky should not reveal the presence of a cluster. From the radial distribution of emission line galaxies, we know that they do not show the cluster as well as the absorption line galaxies. Figures 9 and 10 show the distribution of bright ( $M_{K_s} \leq -22.7 + 5\log h$ ) emission line and absorption line galaxies on the sky. Indeed, the emission line galaxies are much less clustered than absorption line galaxies. It is evident, however, that the emission-line galaxies trace at least some of the same structures, although there are large cluster-to-cluster variations (contrast Coma/A2199/A1367 with A119/A194). It is again striking that the kinematics of the populations are so similar while their spatial distributions differ dramatically. Such a situation is possible if the emission-line galaxies are not in dynamical equilibrium, which would not be surprising for a population on first or second infall.

#### 3.5. Spectroscopic Types as a Function of Local Density

When determining the impact of environment on galaxy properties, it is critical to distinguish between local and global density. We now ask whether the radial dependence of the fraction of galaxies with emission lines is evident when studying this fraction as a function of local galaxy density. Here, we consider the density estimate  $\Sigma_n = n/(\pi D_n^2)$  where  $D_n$  is the projected distance to the  $n$ th nearest neighbor ( $M_K \leq -22.7$ ). We use redshifts to determine cluster membership but not the estimated line-of-sight separation; for cluster members,  $D_n$  is the distance to the  $n$ th nearest member ( $M_K \leq -22.7$ ), but for nonmembers,  $D_n$  is the distance to the  $n$ th nearest galaxy with  $\Delta v \leq 1000 \text{ km s}^{-1}$  ( $M_K \leq -22.7$ ) regardless of cluster membership. The distances  $D_n$  may be underestimated for field galaxies close to the infall regions (where galaxies in the infall region have large peculiar velocities and are therefore counted as neighbors), but such galaxies comprise a small fraction of the total field sample. We restrict the field galaxies to the redshift range  $2000\text{--}12000 \text{ km s}^{-1}$ . We exclude galaxies in the foreground or background of A119, A168, and A194 from the field sample because these systems comprise a large fraction of the foreground or background of the others. Although not a complete sample, the absolute magnitude distribution of the field sample is very similar to the distribution of the

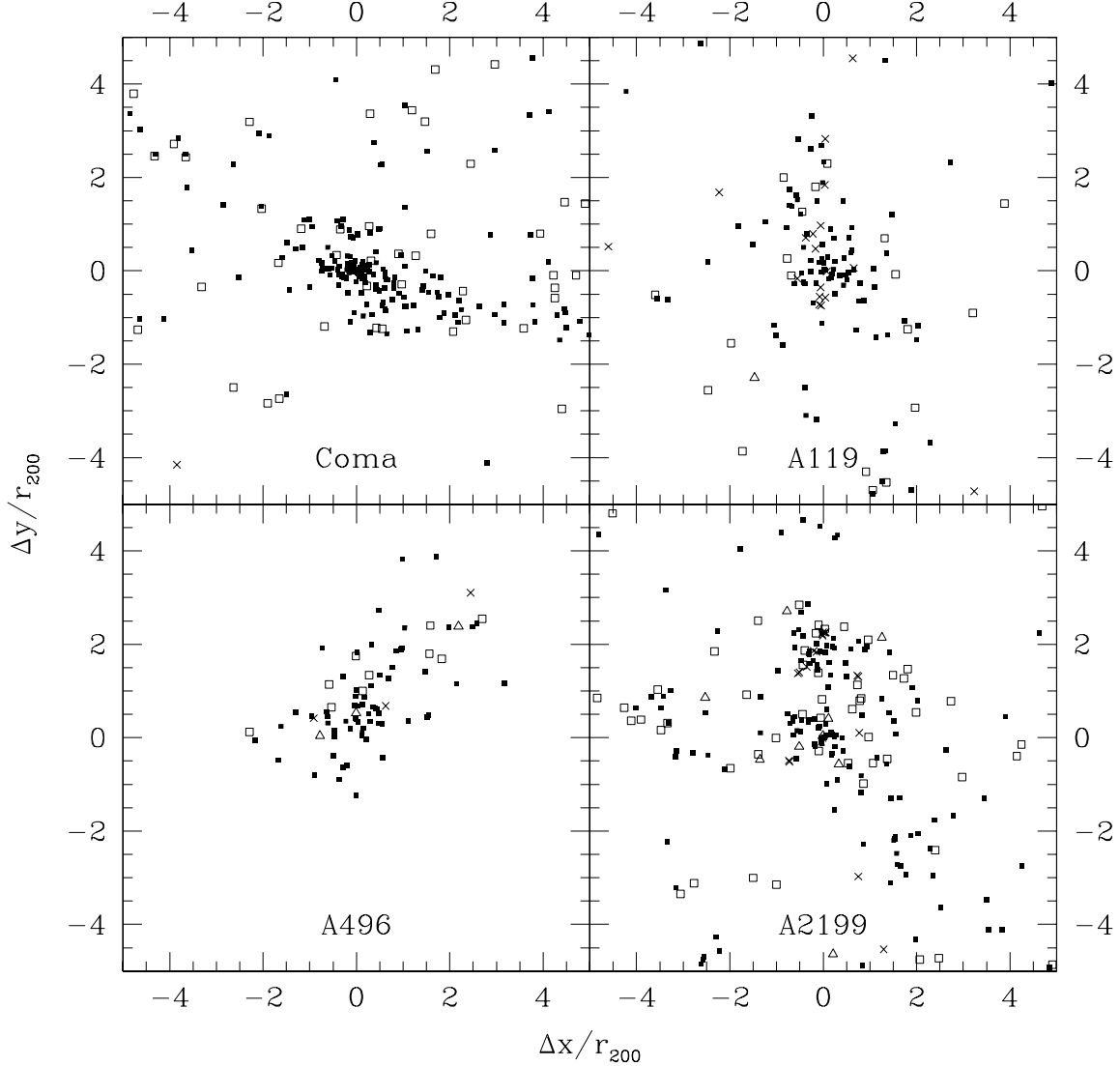


FIG. 9.— Distribution on the sky of different galaxy types in four of the CAIRNS clusters. Solid squares, open squares, and open triangles show absorption-dominated, star-forming, and AGN galaxies respectively, while crosses indicate galaxies without FAST spectra.

cluster/infall sample. We exclude all galaxies for which  $D_n$  is larger than the distance to the edge of the survey region. Because CAIRNS probes rich clusters, we probe densities up to an order of magnitude larger than studies based on 2dF and SDSS (which at present contain relatively few rich, nearby clusters).

Figure 11 shows the fraction of emission-line galaxies as a function of local density ( $\Sigma_5$ ). The trends are very similar to those in Figure 1, demonstrating that local density is indeed an important characterization of environment. Figures 1 and 11 are the only ones which include galaxies fainter than  $M_{K_s} = -22.7 + 5\log h$ , but note that the local density estimate uses only galaxies brighter than this limit (the local densities are therefore directly comparable). In particular, it is curious that A168 shows a stronger trend with local density than with distance from the cluster center. The galaxy samples used to calculate the emission line fraction differ for the different clusters, but the local density  $\Sigma_5$  is always calculated only from the bright galaxies

( $M_K \leq -22.7$ ).

We now test whether local or global environment is more important in determining the star formation properties of the inner parts of galaxies. Figure 12 shows the local density  $\Sigma_5$  as a function of clustrocentric distance. These two parameters are significantly correlated inside  $r_{200}$ , but beyond  $r_{200}$  (the infall regions), there is a wide range of  $\Sigma_5$  at a given value of  $R_p$ . Thus, if clustrocentric radius is more important than local density, the emission fraction of galaxies in the infall region should exhibit little or no dependence on  $\Sigma_5$ .

We separate the galaxies into three types of global environment in Figure 13. The three panels show the emission line fractions of bright galaxies inside the virial regions ( $R_p \leq R_{200}$ ), inside the infall regions ( $1 < R_p/R_{200} \leq 5$ ) and “field” galaxies (all nonmembers with the absolute magnitude and redshift cutoffs described above). At fixed local density, the emission line fraction is independent of global environment (virial region, infall region, or field).

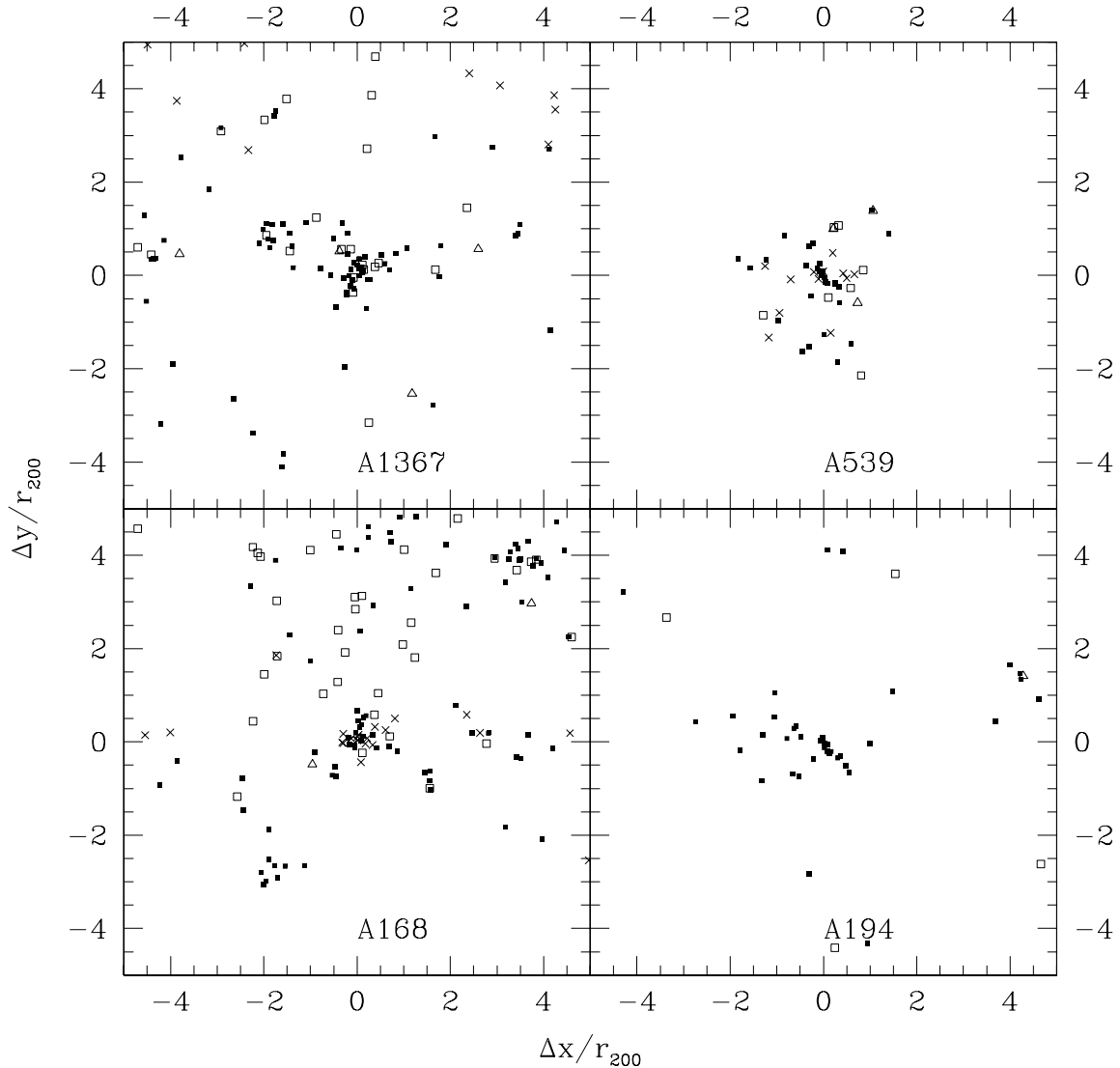


FIG. 10.— Same as Figure 9 for the other CAIRNS clusters in the sample.

This result demonstrates that local density is the primary environmental factor in determining the current star formation properties of galaxies. This conclusion is consistent with previous investigations of galaxies in and near clusters (Balogh et al. 1997; Diaferio et al. 2001; Ellingson et al. 2001; Lewis et al. 2002; Gómez et al. 2003; Treu et al. 2003; Balogh et al. 2004; Gray et al. 2004; Tanaka et al. 2004), and the emission fractions agree well with Balogh et al. (2004). We extend this relation to densities larger by a factor of a few than those probed in Balogh et al. (2004). The emission fraction of galaxies in the virial region declines significantly at densities  $\Sigma_5 \gtrsim 20h^2\text{Mpc}^{-2}$ , a regime previously unprobed (Figure 13).

The strong trend in the field sample (bottom panel of Figure 13) is perhaps surprising, as most previous studies restrict their samples to galaxies in and near clusters and groups where the local density is thought to be more reliable. This dependence probably indicates that there are some galaxy groups in the field sample (we only exclude galaxies in cluster infall regions from the field sample, so

these galaxies should sample a variety of environments). Carter et al. (2001) find a similar trend in the 15R survey (where galaxies are not selected by environment), again indicating the importance of local density. This dependence complicates the determination of the emission line fraction of field galaxies. A similar result was noted by Mateus & Sodr  (2004), who found that the environmental dependence of the emission-line fraction continues to very low densities.

#### 4. ENVIRONMENTAL DEPENDENCE OF STAR FORMATION RATES

In the previous section we showed that the fraction of galaxies with current star formation is dramatically reduced in and around clusters. To find the mechanism driving this reduction in star formation rates we now analyze the star formation rates of cluster galaxies with current star formation. For instance, if the reduction in star formation rates is a gradual process such as starvation, we expect the distribution of star formation rates in cluster

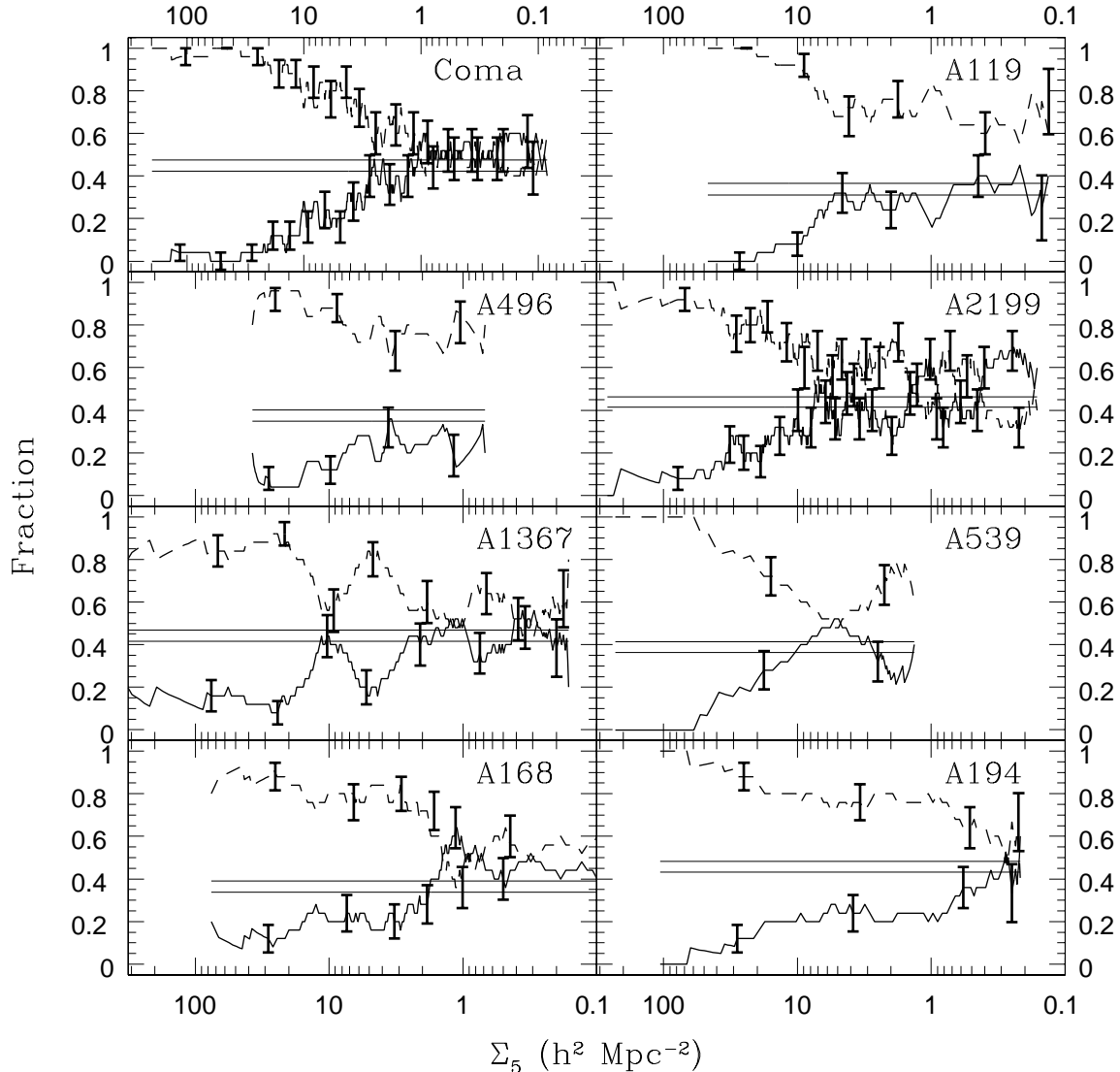


FIG. 11.— Fraction of galaxies with (solid lines) and without (dashed lines)  $H\alpha$  emission as a function of local density  $\Sigma_5$ , the projected density of galaxies (see text). The samples for each cluster are selected by absolute magnitude ( $M_{K_s} \leq M_{K_s,comp}$ ) with a slightly different limit for each cluster. As in Figure 1, the lines show moving averages for bins of 25 galaxies with errorbars indicating independent bins.

galaxies to be skewed to lower rates than in field galaxies (of similar luminosities) with current star formation.

Figure 14 shows  $EW[H\alpha]$  versus clustrocentric radius for galaxies in the  $K_s$  selected samples. Different points show galaxies with absorption lines, AGN, and star formation. Naively, one might expect that the distribution would be contained in a triangular envelope with small EWs at small radii. Instead, galaxies with strong emission lines are present at all radii. These galaxies may be recent arrivals which have not yet been stripped or they may be infall interlopers (§3.1).

Figure 15 shows the distribution of  $EW[H\alpha]$  versus absolute magnitude for galaxies in three types of environment: cluster virial regions, cluster infall regions, and the field. Consistent with many other studies, fainter galaxies tend to have stronger emission lines. CAIRNS virial regions contain few galaxies with strong emission lines. The distribution of  $EW[H\alpha]$  for galaxies in the CAIRNS in-

fall regions, however, is very similar to that in the field. It is curious that the only emission-line galaxies brighter than  $M_{K_s} = -25$  in *any* environment are the cD galaxies of A496 and A2199, both of which are AGN. Figure 16 shows histograms of  $EW[H\alpha]$  in these three environments both for all bright galaxies and for only bright galaxies with  $EW[H\alpha] > 2\text{\AA}$ . We use K-S tests to test whether the distributions of  $EW[H\alpha]$  in the cluster, infall, and field samples are different. The overall bright galaxy samples in the three environments are definitely different (a K-S test distinguishes them with more than 99.9% confidence). Among bright galaxies with emission lines, however, we find no significant differences (at the 90% confidence level) between samples with the same absolute magnitude limits. Similarly, we find no differences among the three environments for galaxies with moderately strong ( $EW[H\alpha] > 10\text{\AA}$ ) emission lines. This weak dependence of  $EW[H\alpha]$  on environment was first observed by Carter et al. (2001) for

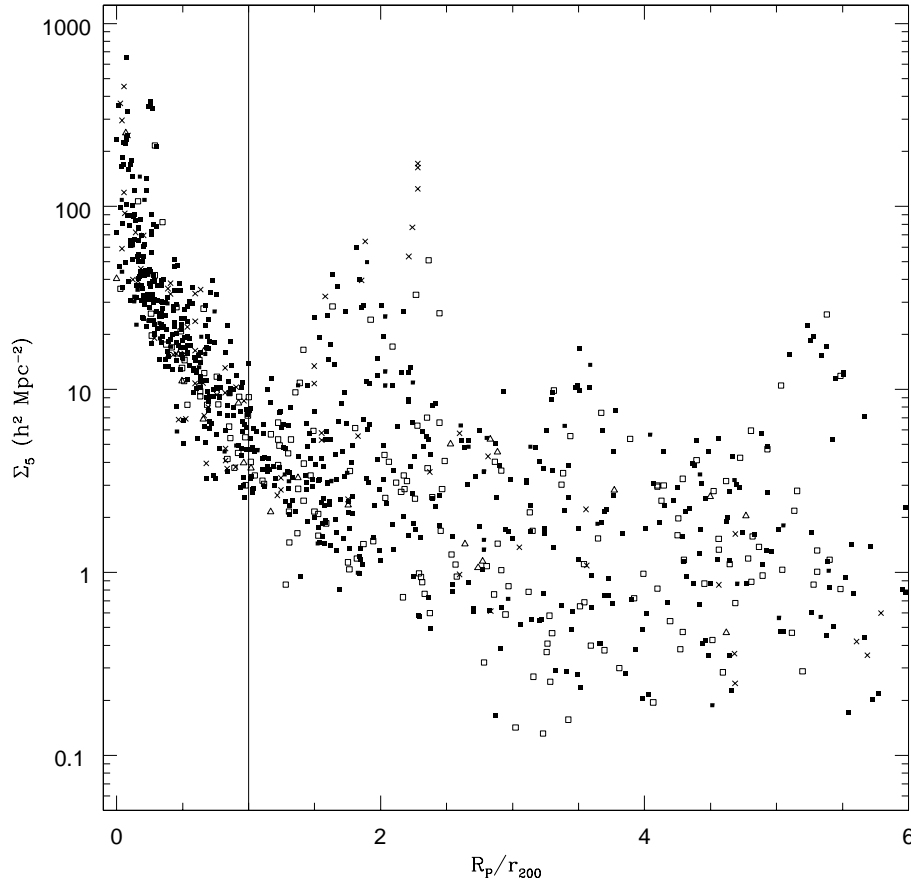


FIG. 12.— Local density  $\Sigma_5$  versus clustercentric radius of bright ( $M_{K_s} \leq -22.7$ ) galaxies in all CAIRNS clusters. Solid squares, open squares, and open triangles show absorption-dominated, star-forming, and AGN galaxies respectively, while crosses indicate galaxies without FAST spectra. The vertical line at  $R_{200}$  separates the virial region from the infall region.

galaxies in all environments from the 15R survey, and this weak dependence has been confirmed by Balogh et al. (2004) and Tanaka et al. (2004), who find similar results in a study of galaxies in both 2dFGRS and SDSS.

One potential explanation of the similarity of the distributions of  $\text{EW}[\text{H}\alpha]$  in different environments is that changes in star formation rates occur abruptly, perhaps due to ram pressure stripping or strong tidal interactions (van Dokkum et al. 1998; Balogh et al. 2004). Galaxies with star formation that is truncated abruptly should show evidence of a population of A stars, i.e., K+A or E+A galaxies (e.g., Kauffmann et al. 2004). We search for galaxies with strong Balmer absorption ( $\text{EW}[\text{H}\delta] > 5\text{\AA}$ ) and find two candidates among  $\approx 1000$  bright galaxies and one definite E+A in A168 at 0.3 mag below our minimum luminosity. Curiously, this galaxy lies just  $23h^{-1}\text{kpc}$  in projection from and at the same redshift as a bright galaxy in our sample that is 2.15 mag brighter than the E+A galaxy. Both of the bright candidates are consistent with  $\text{EW}[\text{H}\delta] \leq 5\text{\AA}$  at the  $1\text{-}\sigma$  level and one of them has a SDSS spectrum which shows emission lines. The frequency of E+As among bright galaxies in nearby clusters is therefore  $\lesssim 0.1\%$ , crudely consistent with other studies of local galaxies in all environments (Zabludoff et al. 1996; Quintero et al. 2004). The FAST spectra have lower S/N

at blue wavelengths. It is thus possible that we miss some of these galaxies due to low S/N. A definitive search would require followup spectra with higher S/N. However, other investigators have found that Coma contains no bright post-starburst/post-star-forming galaxies, unlike clusters at moderate redshift (Caldwell & Rose 1997; Poggianti et al. 2004), although Coma does contain some faint post-starburst galaxies (Caldwell et al. 1996).

Kauffmann et al. (2004) show that the relations between star formation tracers do not depend on environment, despite the fact that the tracers are sensitive to different timescales of star formation. They conclude that the only way to maintain these relations is for cessation of star formation to occur on very long timescales ( $\gtrsim 1$  Gyr). However, this conclusion is based on a specific star formation history where star formation is constant for 10 Gyr ( $\log(SFR/M_*) = -10$  where  $M_*$  is the total stellar mass of the galaxy) after which star formation halts abruptly. This model is reasonable for all emission-line galaxies except those with  $\log M_* \gtrsim 10$  (Brinchmann et al. 2004). However, our sample and that of Balogh et al. (2004) consists mostly of galaxies with these high masses. Brinchmann et al. (2004) find that galaxies with  $\log M_* > 10.5$  typically have  $\log(SFR/M_*) \leq -10.5$ , indicating that their SFRs were greater in the past. Detailed modeling of the

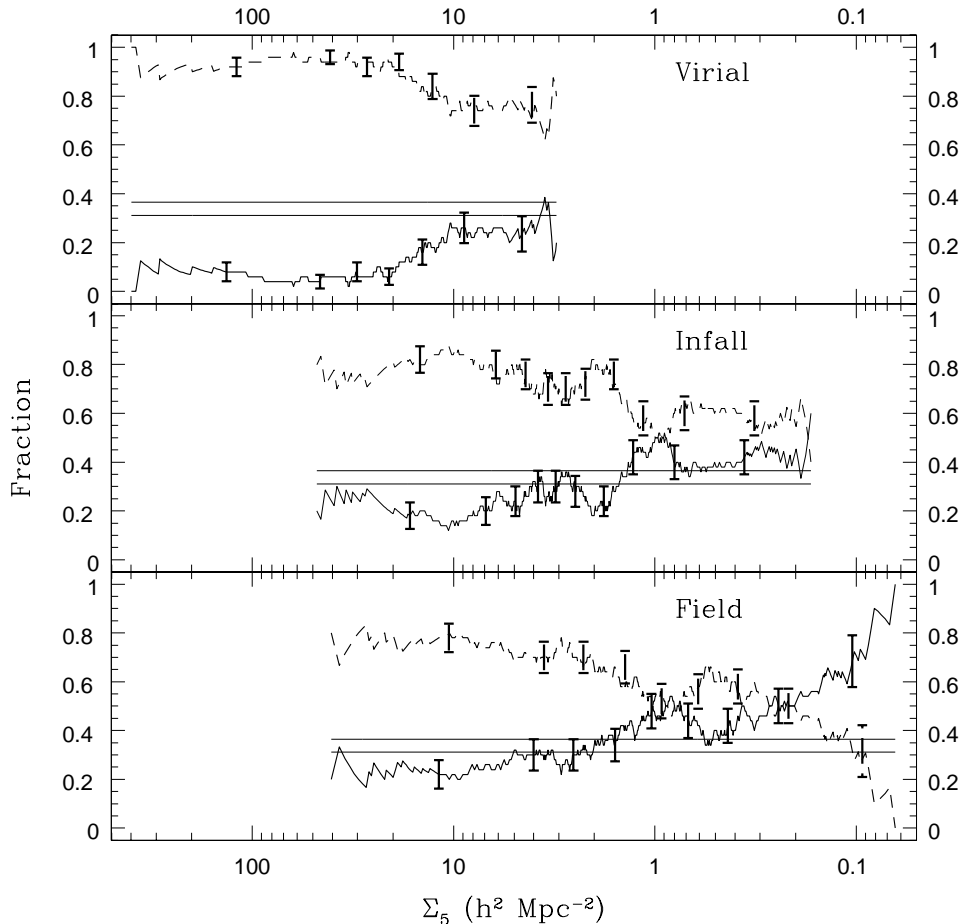


FIG. 13.— Fraction of bright ( $M_{K_s} \leq -22.7$ ) galaxies with (solid lines) and without (dashed lines)  $H\alpha$  emission as a function of local density  $\Sigma_5$ , the projected density of galaxies (see text). As in Figure 1, the lines show moving averages for bins of 25 galaxies with errorbars indicating independent bins.

star formation histories of more massive galaxies may resolve this discrepancy.

The models shown by Kauffmann et al. (2004) reach the SF relations of normal galaxies after  $\sim 1.5$  Gyr. Thus, if cessation of star formation (by any mechanism) occurs largely at moderate or high redshifts (an alternative suggested by Balogh et al. 2004), these galaxies would have sufficient time to reach the SF relations observed for local galaxies. This type of solution points towards the significance of the initial conditions of galaxy formation and thus blurs the line between effects related to the initial conditions of galaxy formation and effects related to subsequent environmental evolution. Detailed studies of  $H\alpha$  properties at moderate redshift should help resolve this conflict. For instance, Kodama et al. (2004) use narrowband imaging and photometric redshifts to analyze one cluster at  $z \approx 0.4$  and find results similar to those we find for clusters in the nearby universe: the fraction of galaxies with  $H\alpha$  emission depends strongly on local density, but the  $H\alpha$  luminosity function does not depend strongly on environment. These results, particularly if they are true generally for clusters at moderate redshift, strengthen the case for rapid truncation of star formation. Curiously, the star formation-density relation in this cluster is much stronger than the morphology-density relation discussed in Treu

et al. (2003), suggesting that star formation is more sensitive than morphology to environment.

Alternatively, there may be competing processes affecting star formation, e.g., reduced star formation due to stripping of the halo gas reservoir but enhanced circumnuclear star formation due to tidally induced starbursts. Because fiber spectra and our FAST spectra are dominated by light from the inner few kpcs of galaxies, these spectra may have larger measured  $EW[H\alpha]$  than integrated spectra (see the discussion in §5). An objective prism study of cluster galaxies suggests that cluster galaxies have a higher incidence of tidally induced circumnuclear starbursts than field galaxies (Moss & Whittle 2000). Detailed modeling would be required to see whether such competing processes would cause galaxies to deviate significantly from the relations among SF tracers. Finally, the importance of projection effects especially for emission-line galaxies (§3.1) suggests that many, perhaps most emission-line galaxies lie at much lower spatial densities. The similarity of the two SFR distributions would then be a consequence of drawing from the same parent distribution of local spatial density and artificially large projected densities.

We now test other density estimators to determine whether suppression of star formation might be correlated with a more local density estimate. We consider four density



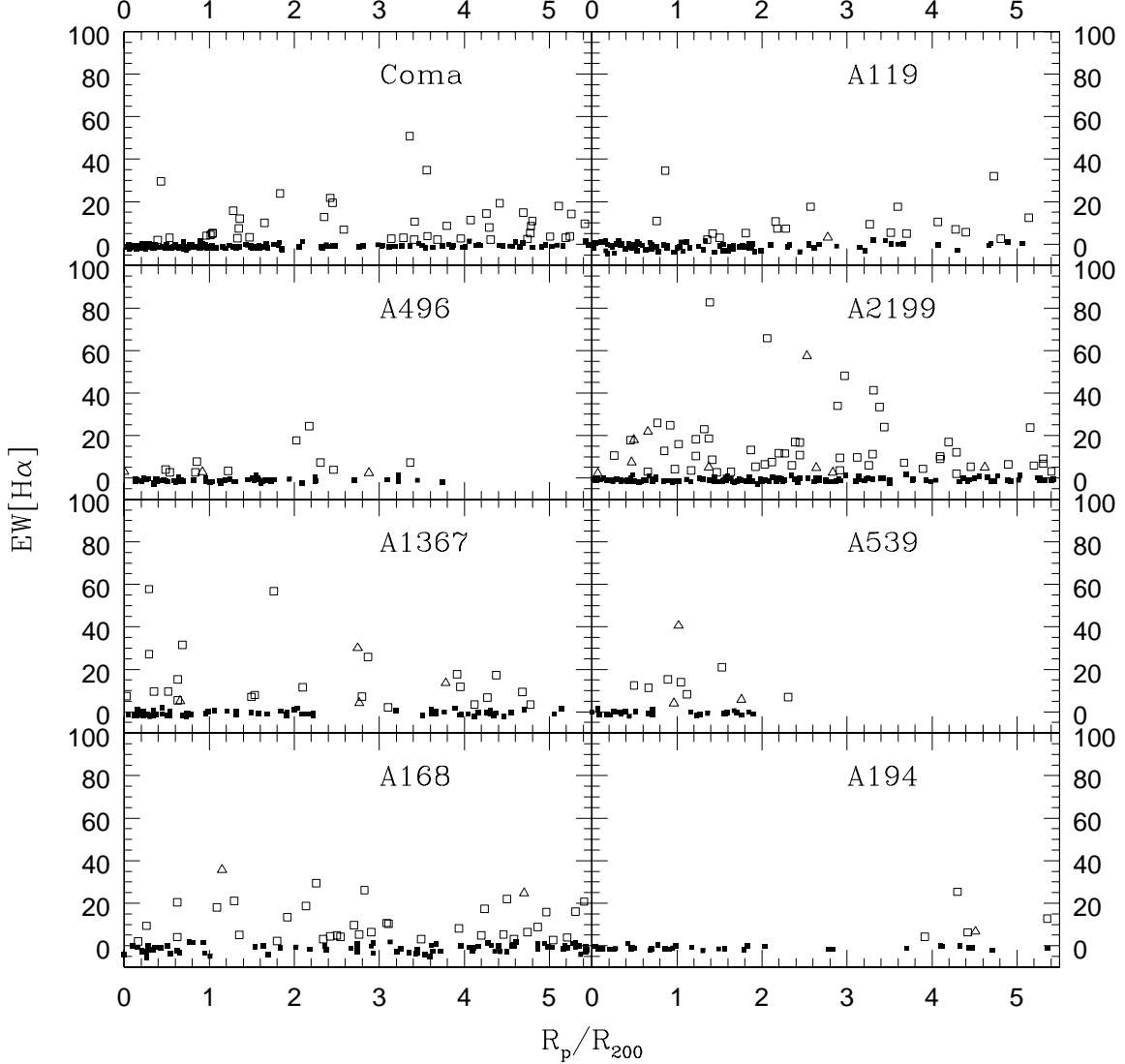


FIG. 14.— EW[H $\alpha$ ] versus clustrocentric radius. Solid squares, open squares, and open triangles show absorption-dominated, star-forming, and AGN galaxies respectively.

estimates: the distance  $D_n$  to the  $n$ th nearest neighbor ( $M_K \leq -22.7$ ) for  $n = 1, 5$ , and 10 (defined in §3.5), and the number of galaxies  $N_{1.1}$  within a circle of radius  $1.1h^{-1}\text{Mpc}$ . Figure 17 shows EW[H $\alpha$ ] as a function of the distance to the nearest (bright) neighbor in the CAIRNS clusters. We exclude all galaxies with  $D_1$  is larger than the distance to the edge of the survey region. Figure 18 shows this relation in three environments: virial regions, infall regions, and the field. Because of the large (projected) densities in the virial regions, there are few “isolated” galaxies in the virial regions with large values of  $D_1$ . Also, “close pairs” (i.e.,  $D_1 \lesssim 50 h^{-1}\text{kpc}$ ) in virial regions contain few galaxies with large EW[H $\alpha$ ] compared to close pairs in infall regions and the field. The close pairs in the infall and field environments with large EW[H $\alpha$ ] ( $>40\text{\AA}$ ) are likely tidally induced starbursts (Barton et al. 2000). Apart from this difference, the distribution of EW[H $\alpha$ ] versus  $D_1$  appears to be very similar in the three environments. Figures 19 and 20 show the similar distributions of EW[H $\alpha$ ] versus

$D_5$ . We find similar distributions of EW[H $\alpha$ ] versus  $D_{10}$  and  $N_{1.1}$  which we omit for brevity. There are no obvious differences in these distributions among the three types of environment. We confirm this quantitatively by comparing the distributions of EW[H $\alpha$ ] for cluster and infall region galaxies above and below the median value of  $D_1$  and  $D_5$  with a K-S test; the tests show no differences at the 95% confidence level. We similarly find no differences in the distributions of EW[H $\alpha$ ] for galaxies in the most and least dense quartiles.

Several authors have discussed the median and quartiles of the distribution of EW[H $\alpha$ ] as a function of local density (Gómez et al. 2003; Balogh et al. 2004; Tanaka et al. 2004). They find evidence for a “break” in the distributions at a local density of  $\Sigma_5 \approx 2h^2\text{Mpc}^{-2}$ . Balogh et al. (2004) notes that this break reflects the local density where the emission-line fraction drops below 25% or 50%. Figure 21 shows the quartiles of the EW[H $\alpha$ ] distribution as a function of local density for the CAIRNS galaxies in

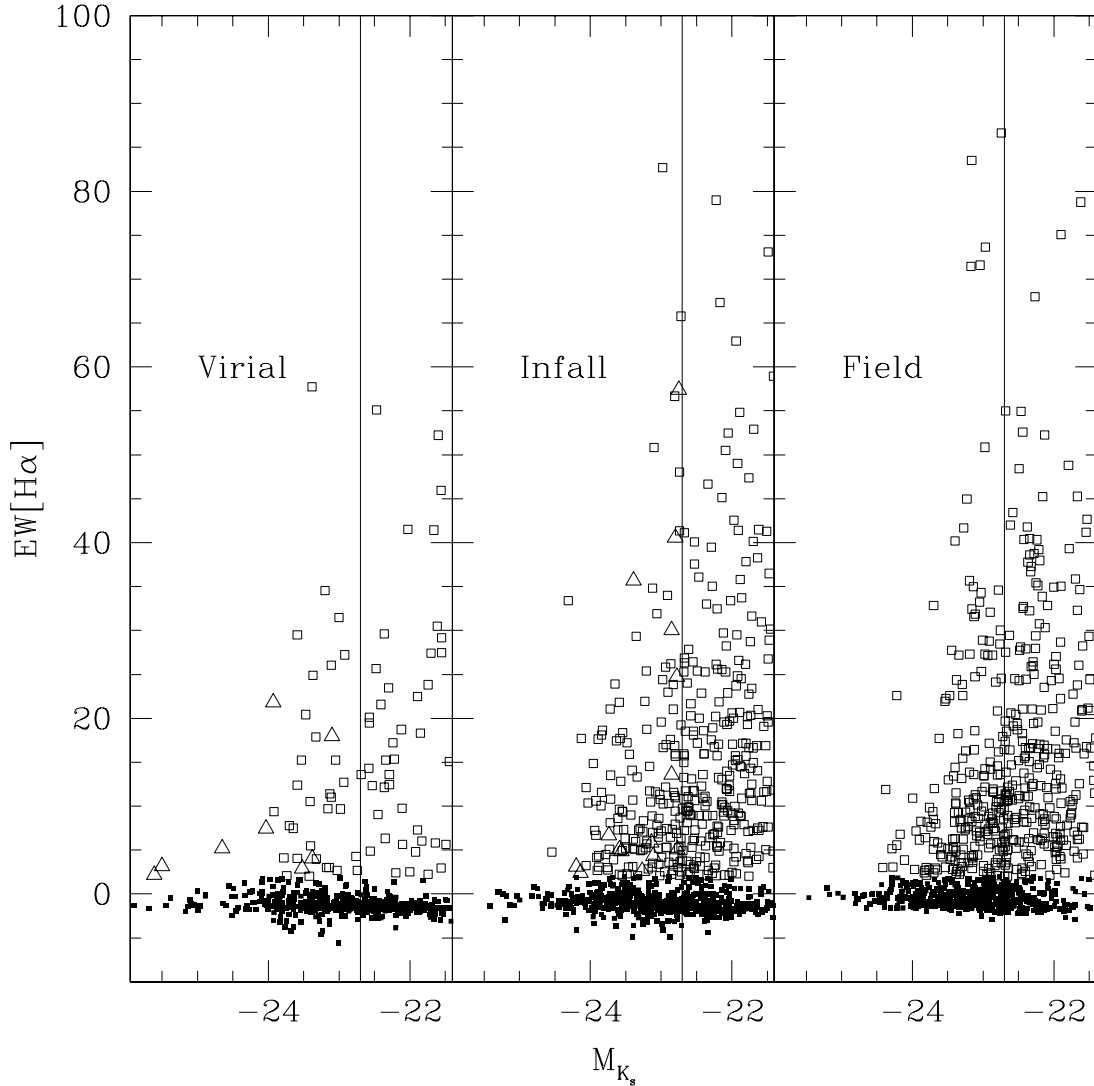


FIG. 15.—  $EW[H\alpha]$  versus absolute magnitude (from left to right) for galaxies in cluster virial regions, infall regions, and the field. Solid squares, open squares, and open triangles show absorption-dominated, star-forming, and AGN galaxies respectively. Vertical lines indicate the spectroscopic completeness limit of the CAIRNS clusters.

the three global environment types (virial regions, infall regions, and field). We confirm that the upper quartile shows a break at  $\Sigma_5 \approx 1 - 2h^2 Mpc^{-2}$ . The quartiles of  $EW[H\alpha]$  for the  $K$ -selected CAIRNS galaxies are similar to those of the red-selected SDSS galaxies in Balogh et al. (2004) and Tanaka et al. (2004) and smaller than those of the blue-selected 2dFGRS galaxies in Balogh et al. (2004). A striking feature of Figure 21 is that the quartiles show a similar dependence on  $\Sigma_5$  in all three environment types. This result further strengthens the case for the primacy of local density in determining galaxy properties.

##### 5. DISCUSSION

We confirm and extend recent results on the environmental dependence of star formation. Our study utilizes a complete, near-infrared sample of cluster galaxies in clusters with robustly determined parameters. Our near-infrared selection yields a sample that is much closer to a sam-

ple selected by stellar mass than samples selected at optical wavelengths. In optically selected samples, the stellar masses of star forming galaxies near the survey limit are smaller than the stellar masses of galaxies near the survey limit without star formation. Thus, near infrared selection significantly reduces this potential systematic bias.

Our galaxy spectra are obtained with long-slit observations, which are relatively insensitive to aperture bias (Carter et al. 2001). However, our spectra are still heavily weighted towards the nuclear regions of galaxies relative to true integrated spectra (e.g., Jansen et al. 2000). This weighting is important to remember when comparing our results to, e.g., detailed studies of Virgo galaxies which show ongoing ram pressure stripping and evidence of truncation of star-forming disks (Koopmann & Kenney 2004; Kenney et al. 2004).

Compared to fiber surveys like 2dFGRS and SDSS, the CAIRNS sample avoids incompleteness due to fiber colli-

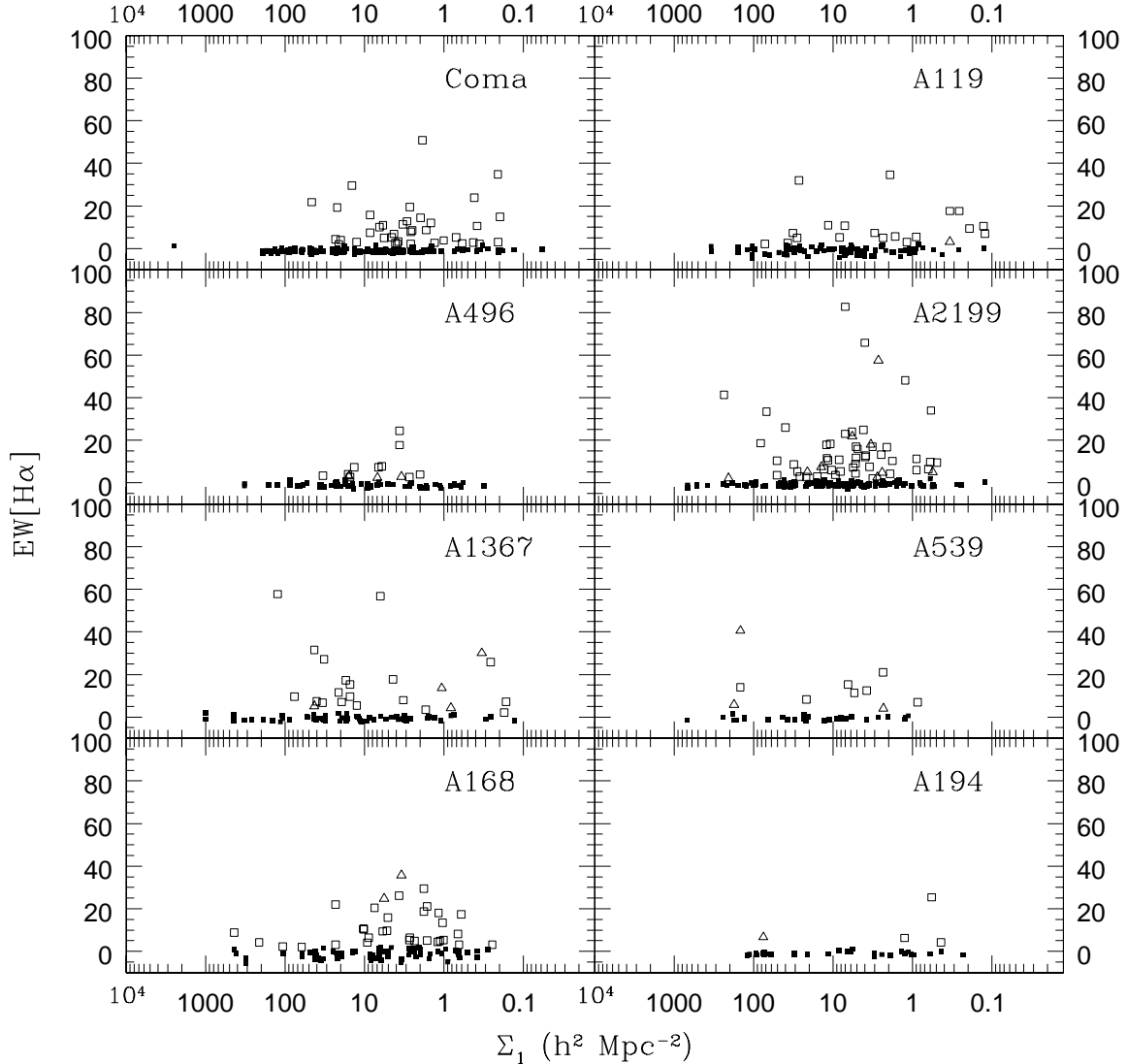


FIG. 17.—  $\text{EW}[\text{H}\alpha]$  versus local density  $\Sigma_1$  (computed from the nearest neighbor distance) for the CAIRNS clusters. Solid squares, open squares, and open triangles show absorption-dominated, star-forming, and AGN galaxies respectively.

sions. This completeness is very important when studying the properties of cluster galaxies with current star formation because these galaxies are quite rare.

Our long-slit spectra are dominated by light from the inner few kpc of galaxies, but they sample some light from the outer parts of galaxies. We therefore expect our results to be more robust to aperture bias than fiber surveys. The consistency of our results with previous investigations suggests that aperture bias and spectroscopic completeness do not cause significant systematic biases in 2dF and SDSS.

A recent study of Virgo spirals (Koopmann & Kenney 2004) suggests an important caveat to the impact of aperture bias on our results. Koopmann & Kenney (2004) find that many Virgo spirals have truncated H $\alpha$  disks (see also Vogt et al. 2004). Because these truncated disks are not often found in samples of field galaxies, estimates of aperture bias based on field samples (Carter et al. 2001; Kewley et al. 2005) may not apply to cluster samples. We attempt to quantify the impact of truncated spirals on our

results. Koopmann & Kenney (2004) list  $\text{EW}[\text{H}\alpha]$  both inside  $r_{24}$  (the R-band isophote of 24 mag arcsec $^{-2}$ ) and inside  $0.3r_{24}$  (their Table 3). From this sample, we find that the ratio  $\text{EW}(\text{inner})/\text{EW}(\text{total})$  is a factor of  $\approx 2.2$  larger for galaxies classified as truncated versus all other galaxies. To estimate the *maximum* impact this truncation would have on our results, we assume that *all* galaxies inside  $R_{200}$  are truncated and that *no* galaxies outside  $R_{200}$  are truncated. Then, a K-S test would detect a difference between the emission-line populations inside/outside  $R_{200}$  (Figure 16) at the 99.8% confidence level. However, some galaxies inside  $R_{200}$  are probably infall interlopers and some galaxies outside  $R_{200}$  are backsplash galaxies. Thus, this estimate is a conservative upper limit on the difference in the two (projected) populations.

Our spectroscopic samples are limited to relatively bright galaxies ( $M \lesssim M^* + 1$ ). Recently, Tanaka et al. (2004) have shown that slightly fainter galaxies ( $1 < M - M^* < 2$ ) in SDSS show different environmental dependencies than

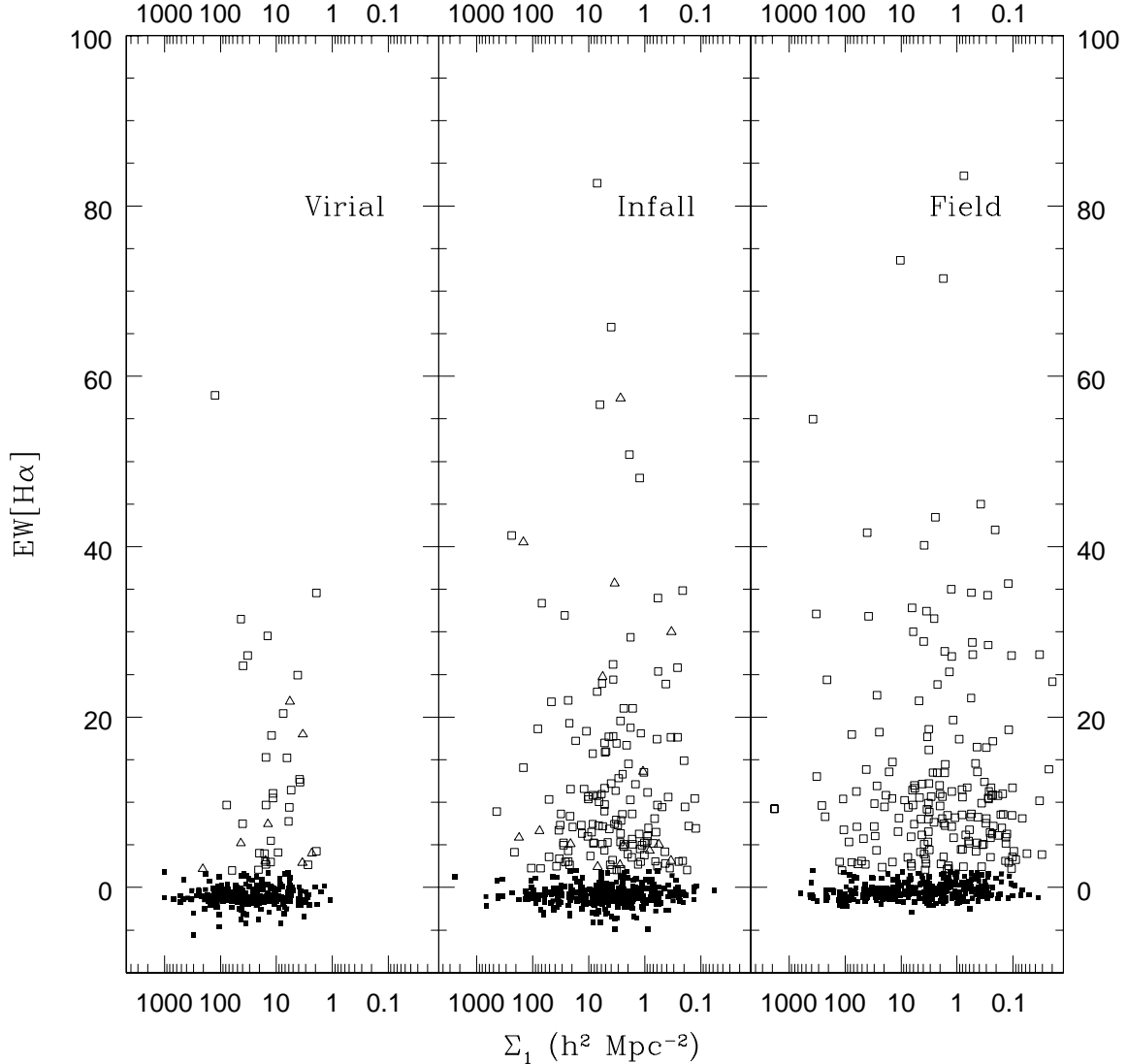


FIG. 18.—  $\text{EW}[\text{H}\alpha]$  versus nearest neighbor distance  $\Sigma_1$  (from left to right) for galaxies in cluster virial regions, infall regions, and the field. Solid squares, open squares, and open triangles show absorption-dominated, star-forming, and AGN galaxies respectively.

bright ( $M \leq M^* + 1$ ) galaxies. The properties of galaxies in the luminosity bin  $1 < M - M^* < 2$  and those of dwarf galaxies are not constrained by our observations.

We measure star formation rates from  $\text{EW}[\text{H}\alpha]$ , similar to many other investigators (Carter et al. 2001; Lewis et al. 2002; Gómez et al. 2003; Balogh et al. 2004; Mateus & Sodr  2004; Tanaka et al. 2004). In assuming  $\text{EW}[\text{H}\alpha]$  is directly proportional to SFR (normalized by galaxy luminosity), we assume that the extinction to continuum and to HII regions are identical. If this assumption is incorrect (Calzetti 2001), then Balmer decrements are necessary to obtain accurate SFR estimates. However, our conclusion that the distribution of  $\text{EW}[\text{H}\alpha]$  among galaxies with current star formation does not depend on environment (§4) holds unless the relative extinctions of continuum and HII regions depend on environment.

## 6. CONCLUSIONS

The environmental dependence of galaxy properties can be decomposed into two effects: the *fraction* of galaxies with current star formation and the *distribution of star formation rates among galaxies with current star formation*. Infall regions (where galaxies are infalling onto the main cluster but have not yet reached equilibrium) provide a unique probe of the size scale on which environment is important: infall regions are overdense on scales of  $5\text{--}10h^{-1}\text{Mpc}$  (because they are near a cluster) but they contain a wide range of local densities measured on scales of roughly  $1h^{-1}\text{Mpc}$ .

The CAIRNS sample confirms that the fraction of galaxies with current star formation is suppressed both inside and outside the virial regions of rich clusters. For the first time, we show this effect in individual clusters as well as cluster-to-cluster variations in the effect. One cluster, A2199, contains X-ray groups at large radii. The emission fraction profile shows a dip at the radius of these groups, indicating that they are sufficiently massive to influence

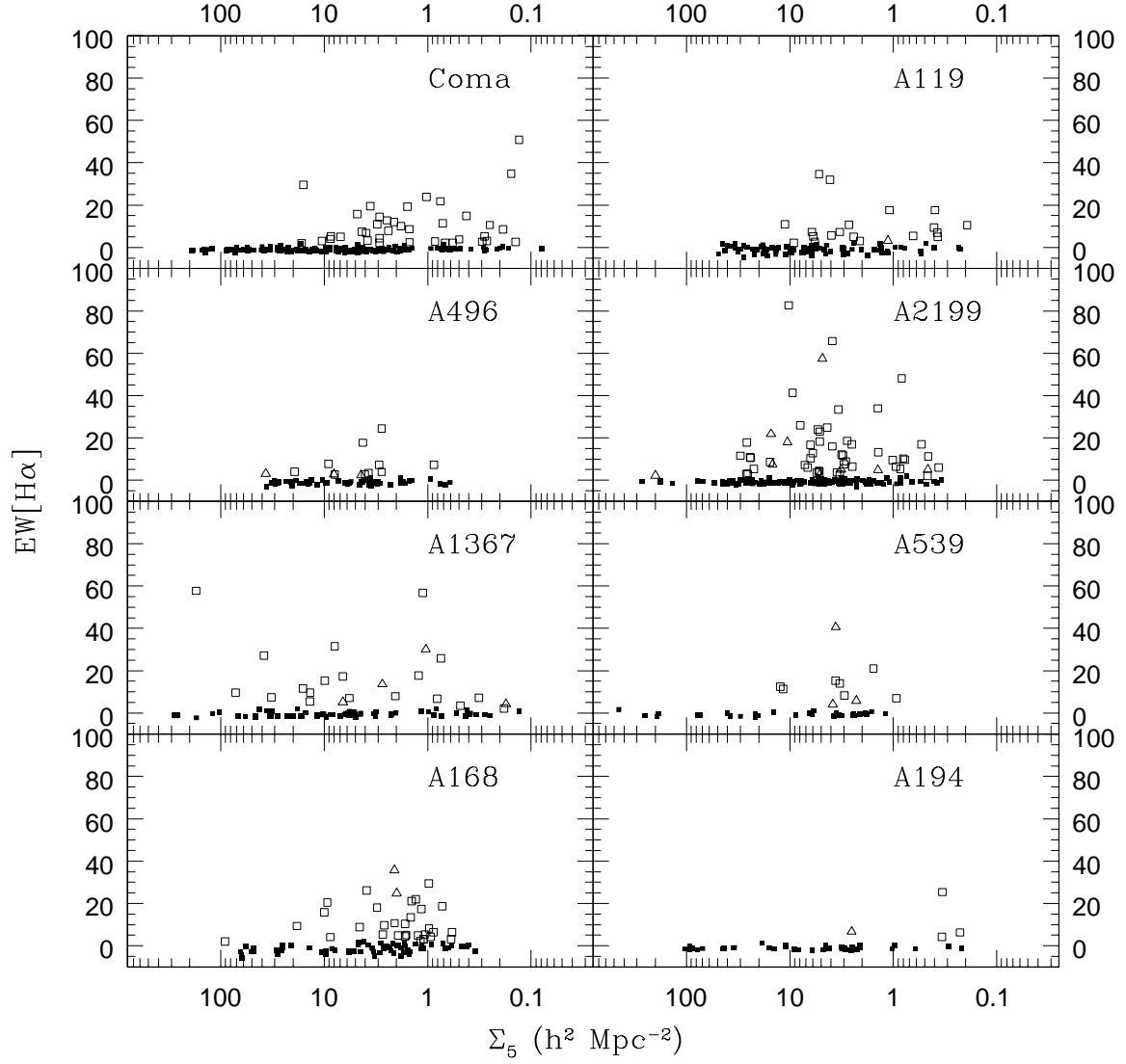


FIG. 19.—  $EW[H\alpha]$  versus  $\Sigma_5$  for the CAIRNS clusters. Solid squares, open squares, and open triangles show absorption-dominated, star-forming, and AGN galaxies respectively.

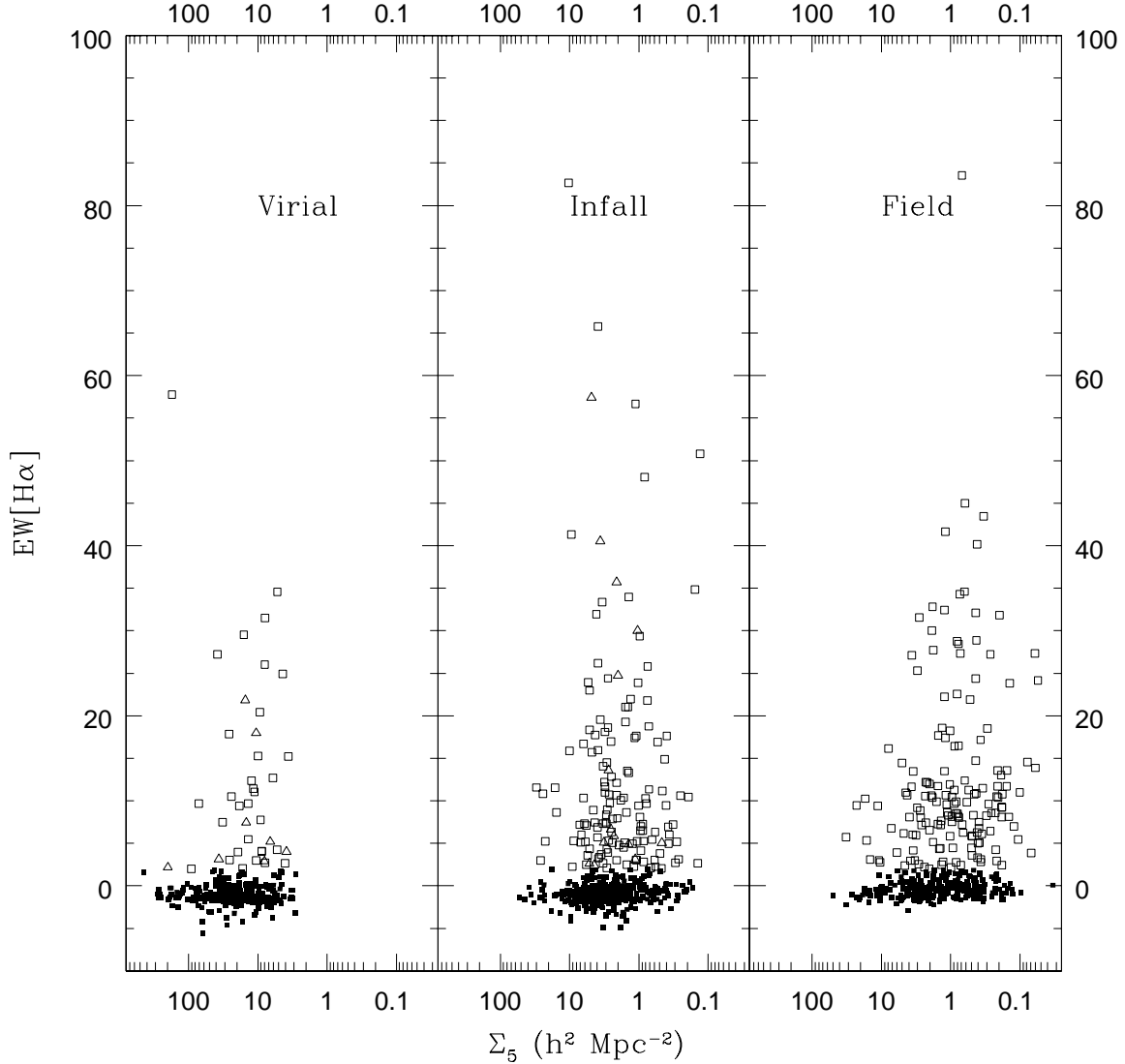


FIG. 20.—  $\text{EW}[\text{H}\alpha]$  versus  $\Sigma_5$  (from left to right) for galaxies in cluster virial regions, infall regions, and the field. Solid squares, open squares, and open triangles show absorption-dominated, star-forming, and AGN galaxies respectively.

galaxy properties. More generally, the emission-line fraction depends strongly on local projected galaxy density, and this dependence is the same in different types of global environment (virial regions, infall regions, and the field). These results together suggest a limited role for cluster-specific mechanisms. We extend this spectral type-density relation to higher local densities than probed by 2dF and SDSS (which at present contain relatively few rich, nearby clusters). Our results indicate that previous studies based on 2dF and SDSS data have not been biased by systematic effects due to fiber spectra, aperture bias, or incompleteness in dense regions.

The radial distribution of both emission-line and absorption-line galaxies closely follow NFW profiles, but with very different concentrations,  $c \approx 4.3$  and  $0.8$  for absorption and emission-line galaxies respectively. Both concentrations are smaller than the mass profiles in Paper I. Lin et al. (2004) reached similar conclusions about the relative distributions of galaxies and dark matter. From these profiles

we can predict the rate of “infall interlopers,” galaxies with  $R_p \leq r_{200}$  but  $r_{3D} > r_{200}$ . At least 20% of absorption line galaxies and 50% of emission line galaxies are infall interlopers. Departures from spherical symmetry would likely increase the fraction of emission-line galaxies which are infall interlopers.

Our spectroscopic completeness is important for studying the kinematics of galaxies with and without emission lines. There is little evidence for kinematic segregation between the two populations within the virial radius  $r_{200}$ , contrary to previous results and conventional wisdom. We show that kinematic segregation is a very subtle issue strongly dependent on membership classification, survey depth and completeness, parametric versus nonparametric tests, and galaxy classification.

Galaxy populations vary with environment both inside and outside cluster virial regions. Galaxies in cluster infall regions are an intermediate population between cluster galaxies and field galaxies. Thus, either the physical

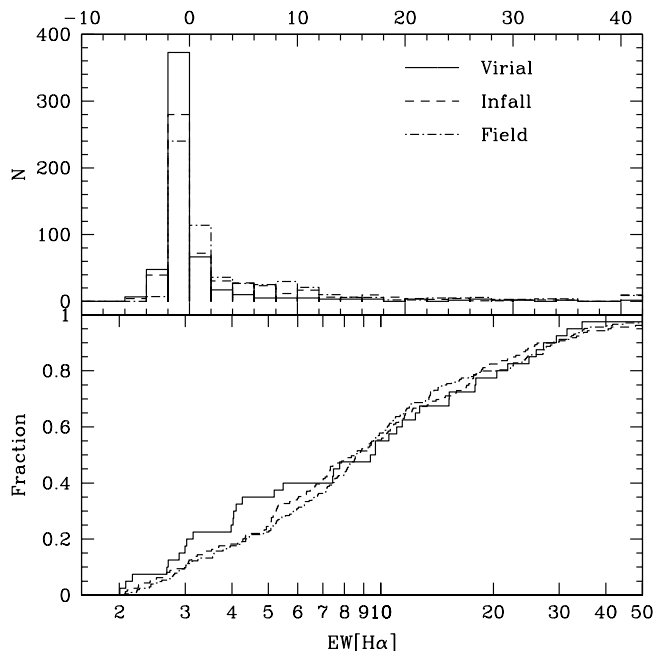


FIG. 16.— (Top panel) Distribution of EW[H $\alpha$ ] in different environments. Solid, dashed, and dash-dotted lines indicate galaxies in virial regions, infall regions, and the field respectively. Histograms have been normalized to have equal areas. (Bottom panel) Cumulative distributions of EW[H $\alpha$ ] for galaxies with EW[H $\alpha$ ]  $\geq 2\text{\AA}$ .

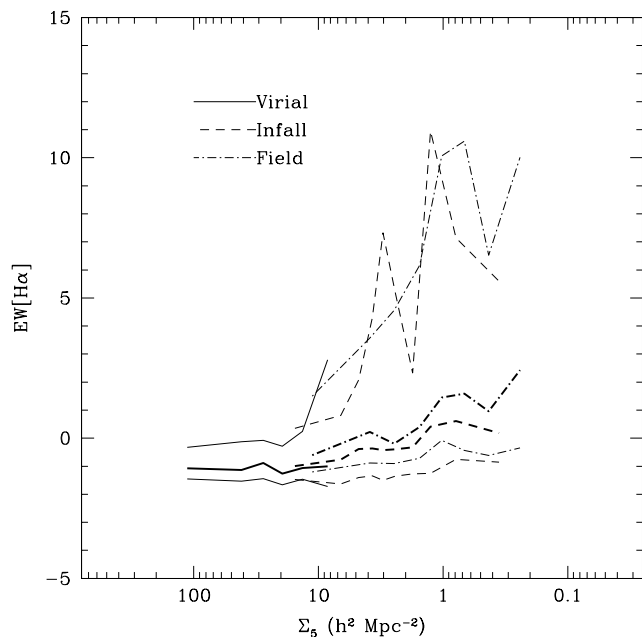


FIG. 21.— Medians (thick lines) and quartiles (thin lines) of the distributions of EW[H $\alpha$ ] versus local density  $\Sigma_5$  in the three global environment types.

mechanisms responsible for changes in galaxy populations operate outside of cluster virial regions or a significant number of galaxies in the infall region have already passed through the virial region. The latter “backsplash” scenario has been invoked to explain the presence of galaxies apparently stripped of H I at large distances from clusters.

Numerical simulations predicts different velocity distributions for backplash galaxies and those on first infall in the interval  $1.4 < R_p/r_{200} < 2.8$  (Gill et al. 2005). A toy model of this backplash scenario (where we assume that backplash is the only mechanism affecting star formation and that this mechanism is perfectly efficient) disagrees with the observations. The H I-deficient galaxies may in fact be backplash galaxies, but our result shows that the backplash scenario cannot be the only or even the primary mode of galaxy transformation. This result supports mechanisms for which local galaxy density is more important than the distance to the nearest cluster. This conclusion agrees with the results of previous studies which show similar relations between galaxy population and local density both near and far from clusters (Lewis et al. 2002; Gómez et al. 2003; Balogh et al. 2004; Treu et al. 2003; Tanaka et al. 2004). We confirm that galaxy properties seem to change significantly at local densities larger than  $\Sigma_5 \gtrsim 2h^2 \text{ Mpc}^{-2}$ . It is remarkable that a similar scale has been found in many heterogeneous studies using different wavelengths for selection and different classification schemes (morphological, photometric, or spectroscopic) (Postman & Geller 1984; Lewis et al. 2002; Gómez et al. 2003; Balogh et al. 2004; Treu et al. 2003; Tanaka et al. 2004).

The *distribution* of star formation rates (emission-line strengths in the inner parts of galaxies, to be precise) among galaxies *with current star formation* shows little dependence on environment, confirming previous studies (Carter et al. 2001; Balogh et al. 2004; Tanaka et al. 2004). This result excludes mechanisms which produce gradual reductions in star formation rates and supports those that lead to sudden truncation of star formation (see also van Dokkum et al. 1998; Balogh et al. 2004) or mechanisms (of any timescale) which operate only until moderate redshifts (timescales  $\gtrsim 1.5$  Gyr, see §4 and Kauffmann et al. 2004). If these mechanisms lose effectiveness in more recent times, star-forming galaxies which “survive” until moderate redshift would evolve similarly to star-forming field galaxies; galaxies that lose their gas reservoir evolve until little evidence remains of their earlier star formation. An alternative possibility is that much of the star formation seen in cluster virial and infall regions occurs in bursts with short timescales consistent with tidal triggering (e.g., Barton et al. 2000; Moss & Whittle 2000). Finally, if most emission-line galaxies observed at large projected densities lie at significantly lower spatial densities, the similarity of the distributions is simply a result of looking at two samples of the same parent distribution. From the number density profiles of the two galaxy types, we calculate that at least 50% of emission-line galaxies with  $R_p < r_{200}$  are infall interlopers. Galaxies in infall regions sample a wide range of local densities (Figure 12), so this explanation is plausible.

Our observations (and those of fiber-based surveys) are not very sensitive to H $\alpha$  emission in the galaxy outskirts; thus our spectra will likely not show evidence of truncated star-forming disks (cf. Koopmann & Kenney 2004; Vogt et al. 2004). If star formation in the inner few kpc of galaxies is unaffected on average, then this difference might explain why we find a similar distribution of SFRs inside and outside clusters. Integrated spectra or wide-

field, narrowband H $\alpha$  observations could test this hypothesis. An objective prism study of cluster galaxies suggests that cluster galaxies have a higher incidence of tidally induced circumnuclear starbursts than field galaxies (Moss & Whittle 2000), again indicating differences between the star formation properties of cluster galaxies measured on different size scales even though these differences are not large for field galaxies (Kewley et al. 2005).

Future studies of galaxy properties in poor clusters and groups may provide further insight into the physical mechanisms responsible for the relation between star formation and local galaxy density. Similarly, detailed studies of individual galaxies may show these mechanisms in operation (e.g., Kenney et al. 2004). Extending these observations to systems at moderate and high redshift would directly probe the timescale of this evolution. In a study of a cluster at  $z \approx 0.4$  with narrowband H $\alpha$  photometry, Kodama et al. (2004) find trends similar to those found in the local universe in both the spectral type-density relation and the weak dependence of the H $\alpha$  luminosity function on local density. Finally, H I observations of complete samples of cluster galaxies could reveal the connections between star formation rates and the available gas reservoir (e.g., Vogt et al. 2004). Untangling the relation between and evolution of different tracers of star formation as a function of environment is a difficult proposition, but future observations hold the promise of resolving several of the curious results we find in nearby clusters and their outskirts.

We thank Michael Balogh, Jeff Kenney, and Richard Larson for useful discussions which significantly improved the presentation of this paper. We thank Perry Berlind and Michael Calkins, the remote observers at FLWO, Susan Tokarz, who processed the spectroscopic data, and all FAST queue observers who took data for CAIRNS. MJG and MJK are supported in part by the Smithsonian Institution. This research has made use of the NASA/IPAC Extragalactic Database (NED) which is operated by the Jet Propulsion Laboratory, California Institute of Technology, under contract with the National Aeronautics and Space Administration. This publication makes use of data products from the Two Micron All Sky Survey, which is a joint project of the University of Massachusetts and the Infrared Processing and Analysis Center/California Institute of Technology, funded by the National Aeronautics and Space Administration and the National Science Foundation. We thank the anonymous referee for a careful reading and useful questions and suggestions which improved the presentation of this paper.

#### REFERENCES

- Abell, G. O., Corwin, H. G., & Olowin, R. P. 1989, *ApJS*, 70, 1  
 Abraham, R. G. et al. 1996, *ApJ*, 471, 694  
 Andreon, S. 2002, *A&A*, 382, 495  
 Balogh, M. et al. 2004, *MNRAS*, 348, 1355  
 Balogh, M. L., Morris, S. L., Yee, H. K. C., Carlberg, R. G., & Ellingson, E. 1997, *ApJ*, 488, L75  
 Balogh, M. L., Navarro, J. F., & Morris, S. L. 2000, *ApJ*, 540, 113  
 Barton, E. J., Geller, M. J., & Kenyon, S. J. 2000, *ApJ*, 530, 660  
 Bell, E. F., McIntosh, D. H., Katz, N., & Weinberg, M. 2003, *ApJS*, 149, 289  
 Binggeli, B., Tammann, G. A., & Sandage, A. 1987, *AJ*, 94, 251  
 Biviano, A., Katgert, P., Thomas, T., & Adami, C. 2002, *A&A*, 387, 8  
 Brinchmann, J., Charlot, S., White, S. D. M., Tremonti, C., Kauffmann, G., Heckman, T., & Brinkmann, J. 2004, *MNRAS*, 351, 1151  
 Caldwell, N. & Rose, J. A. 1997, *AJ*, 113, 492  
 Caldwell, N., Rose, J. A., Franx, M., & Leonardi, A. J. 1996, *AJ*, 111, 78  
 Calzetti, D. 2001, *PASP*, 113, 1449  
 Carlberg, R. G. et al. 1997, *ApJ*, 476, L7  
 Carter, B. J., Fabricant, D. G., Geller, M. J., Kurtz, M. J., & McLean, B. 2001, *ApJ*, 559, 606  
 Christlein, D. & Zabludoff, A. I. 2005, *ApJ*, 621, 201  
 Cole, S. et al. 2001, *MNRAS*, 326, 255  
 Colless, M. & Dunn, A. M. 1996, *ApJ*, 458, 435  
 Colless, M. et al. 2001, *MNRAS*, 328, 1039  
 Diaferio, A. 1999, *MNRAS*, 309, 610  
 Diaferio, A., Kauffmann, G., Balogh, M. L., White, S. D. M., Schade, D., & Ellingson, E. 2001, *MNRAS*, 323, 999  
 Dressler, A. 1980, *ApJ*, 236, 351  
 Ebeling, H., Voges, W., Bohringer, H., Edge, A. C., Huchra, J. P., & Briel, U. G. 1996, *MNRAS*, 281, 799  
 Ellingson, E., Lin, H., Yee, H. K. C., & Carlberg, R. G. 2001, *ApJ*, 547, 609  
 Fabricant, D., Cheimets, P., Caldwell, N., & Geary, J. 1998, *PASP*, 110, 79  
 Fukazawa, Y., Makishima, K., Tamura, T., Ezawa, H., Xu, H., Ikebe, Y., Kikuchi, K., & Ohashi, T. 1998, *PASJ*, 50, 187  
 Gómez, P. L. et al. 2003, *ApJ*, 584, 210  
 Gill, S. P. D., Knebe, A., & Gibson, B. K. 2005, *MNRAS*, 356, 1327  
 Godwin, J. G., Metcalfe, N., & Peach, J. V. 1983, *MNRAS*, 202, 113  
 Goto, T. et al. 2003, *PASJ*, 55, 757  
 Gray, M. E., Wolf, C., Meisenheimer, K., Taylor, A., Dye, S., Borch, A., & Kleinheinrich, M. 2004, *MNRAS*, 347, L73  
 Hernquist, L. 1990, *ApJ*, 356, 359  
 Hubble, E. & Humason, M. L. 1931, *ApJ*, 74, 43  
 Huchra, J. P. 1985, in *ESO Workshop on the Virgo Cluster*, 181–200  
 Jansen, R. A., Fabricant, D., Franx, M., & Caldwell, N. 2000, *ApJS*, 126, 331  
 Jarrett, T. H., Chester, T., Cutri, R., Schneider, S., Skrutskie, M., & Huchra, J. P. 2000, *AJ*, 119, 2498  
 Kauffmann, G., White, S. D. M., Heckman, T. M., Ménard, B., Brinchmann, J., Charlot, S., Tremonti, C., & Brinkmann, J. 2004, *MNRAS*, 353, 713  
 Kauffmann, G. et al. 2003, *MNRAS*, 346, 1055  
 Kenney, J. D. P., van Gorkom, J. H., & Vollmer, B. 2004, *AJ*, 127, 3361  
 Kent, S. M. & Gunn, J. E. 1982, *AJ*, 87, 945  
 Kewley, L. J., Dopita, M. A., Sutherland, R. S., Heisler, C. A., & Trevena, J. 2001, *ApJ*, 556, 121  
 Kewley, L. J., Geller, M. J., & Jansen, R. A. 2004, *AJ*, 127, 2002  
 Kewley, L. J., Jansen, R. A., & Geller, M. J. 2005, *PASP*, in press (astro-ph/0501229)  
 Kochanek, C. S., Pahre, M. A., & Falco, E. 2003, *ApJ*, submitted (astro-ph/0011458)  
 Kodama, T., Balogh, M. L., Smail, I., Bower, R. G., & Nakata, F. 2004, *MNRAS*, 354, 1103  
 Koopmann, R. A. & Kenney, J. D. P. 1998, *ApJ*, 497, L75+  
 —. 2004, *ApJ*, 613, 886  
 Kurtz, M. J. & Mink, D. J. 1998, *PASP*, 110, 934  
 Larson, R. B., Tinsley, B. M., & Caldwell, C. N. 1980, *ApJ*, 237, 692  
 Lewis, I. et al. 2002, *MNRAS*, 334, 673  
 Lin, Y., Mohr, J. J., & Stanford, S. A. 2004, *ApJ*, 610, 745  
 Loveday, J. 2000, *MNRAS*, 312, 557  
 Mamon, G. A., Sanchis, T., Salvador-Solé, E., & Solanes, J. M. 2004, *A&A*, 414, 445  
 Mateus, A. & Sodré, L. 2004, *MNRAS*, 349, 1251  
 Mohr, J. J., Geller, M. J., Fabricant, D. G., Wegner, G., Thorstensen, J., & Richstone, D. O. 1996, *ApJ*, 470, 724  
 Moss, C. & Whittle, M. 2000, *MNRAS*, 317, 667  
 Navarro, J. F., Frenk, C. S., & White, S. D. M. 1997, *ApJ*, 490, 493  
 Nikolaev, S., Weinberg, M. D., Skrutskie, M. F., Cutri, R. M., Wheelock, S. L., Gizis, J. E., & Howard, E. M. 2000, *AJ*, 120, 3340  
 Poggianti, B. M. 1997, *A&AS*, 122, 399  
 Poggianti, B. M., Bridges, T. J., Komiyama, Y., Yagi, M., Carter, D., Mobasher, B., Okamura, S., & Kashikawa, N. 2004, *ApJ*, 601, 197  
 Postman, M. & Geller, M. J. 1984, *ApJ*, 281, 95  
 Quintero, A. D. et al. 2004, *ApJ*, 602, 190  
 Regös, E. & Geller, M. J. 1989, *AJ*, 98, 755  
 Rines, K., Geller, M. J., Diaferio, A., Kurtz, M. J., & Jarrett, T. H. 2004, *AJ*, 128, 1078  
 Rines, K., Geller, M. J., Diaferio, A., Mahdavi, A., Mohr, J. J., & Wegner, G. 2002, *AJ*, 124, 1266  
 Rines, K., Geller, M. J., Kurtz, M. J., & Diaferio, A. 2003, *AJ*, 126, 2152



- Rines, K., Geller, M. J., Kurtz, M. J., Diaferio, A., Jarrett, T. H., & Huchra, J. P. 2001a, *ApJ*, 561, L41
- Rines, K., Mahdavi, A., Geller, M. J., Diaferio, A., Mohr, J. J., & Wegner, G. 2001b, *ApJ*, 555, 558
- Salzer, J. J. 1989, *ApJ*, 347, 152
- Sanchis, T., Mamon, G. A., Salvador-Solé, E., & Solanes, J. M. 2004, *A&A*, 418, 393
- Sanchis, T., Solanes, J. M., Salvador-Solé, E., Fouqué, P., & Manrique, A. 2002, *ApJ*, 580, 164
- Schlegel, D. J., Finkbeiner, D. P., & Davis, M. 1998, *ApJ*, 500, 525
- Skrutskie, M. F. et al. 1997, in *ASSL Vol. 210: The Impact of Large Scale Near-IR Sky Surveys*, 25
- Solanes, J. M., Sanchis, T., Salvador-Solé, E., Giovanelli, R., & Haynes, M. P. 2002, *AJ*, 124, 2440
- Stoughton, C. et al. 2002, *AJ*, 123, 485
- Tanaka, M., Goto, T., Okamura, S., Shimasaku, K., & Brinkman, J. 2004, *AJ*, 128, 2677
- Treu, T., Ellis, R. S., Kneib, J., Dressler, A., Smail, I., Czoske, O., Oemler, A., & Natarajan, P. 2003, *ApJ*, 591, 53
- van den Bergh, S. 1976, *ApJ*, 206, 883
- van Dokkum, P. G., Franx, M., Kelson, D. D., Illingworth, G. D., Fisher, D., & Fabricant, D. 1998, *ApJ*, 500, 714
- Veilleux, S. & Osterbrock, D. E. 1987, *ApJS*, 63, 295
- Vogt, N. P., Haynes, M. P., Giovanelli, R., & Herter, T. 2004, *AJ*, 127, 3300
- Zabludoff, A. I., Zaritsky, D., Lin, H., Tucker, D., Hashimoto, Y., Shectman, S. A., Oemler, A., & Kirshner, R. P. 1996, *ApJ*, 466, 104